University of South Bohemia in České Budějovice
Faculty of Science

Bachelor thesis

Hafnium Chloride, an Alternative Staining Reagent for Biological Electron Microscopy

Faculty of Science, University of South Bohemia
Institute of Parasitology, Biology Centre, Laboratory of Electron Microscopy

Magdalena V. Baranyi

2020

Supervised by RNDr. Marie Vancová, Ph.D.

České Budějovice 2020

Baranyi M., 2020: Hafnium Chloride, an Alternative Staining Reagent for Biological Electron Microscopy. Bc. Thesis, in English – 41p, Faculty of Science, University of South Bohemia, České Budějovice, Czech Republic.

Annotation

This study focuses on the staining pattern of the non-radioactive heavy metal EM stain $HfCl_4$, used during freeze substitution specimen preparation. $HfCl_4$ was investigated as an alternative for the prominent uranyl acetate, since uranium based materials have been placed under heavy restrictions and bans worldwide. We have found a strong $HfCl_4$ staining pattern of microtubules in myoepithelial cells of *Ixodes ricinus* salivary glands. Additionally, in several samples, $HfCl_4$ was found to completely fill the cytoplasm of the myoepithelial cells. Nonetheless, artefact formation around granulated cells was also experienced.

Declaration

I hereby declare that I have worked on my bachelor's thesis independently and used only the sources listed in the bibliography.

I hereby declare that, in accordance with Article 47b of Act No. 111/1998 in the valid wording, I agree with the publication of my bachelor thesis, in full to be kept in the Faculty of Science archive, in electronic form in publicly accessible part of the STAG database operated by the University of South Bohemia in České Budějovice accessible through its web pages. Further, I agree to the electronic publication of the comments of my supervisor and thesis opponents and the record of the proceedings and results of the thesis defense in accordance with aforementioned Act No. 111/1998. I also agree to the comparison of the text of my thesis with the Theses.cz thesis database operated by the National Registry of University Theses and a plagiarism detection system.

České Budějovice, 9.12.2020 ……..……...

Magdalena Baranyi

Acknowledgements

Firstly, I would like to express my gratitude towards my thesis supervisor RNDr. Marie Vancová, PhD, for encouraging me throughout my practical work at the Laboratory of Electron Microscopy and her dedication for solving problems that occurred during my laboratory work. Her guidance, constructive comments and patience during the thesis writing process helped me accomplish this project. Additionally, I would like to thank Mgr. Martina Tesařová for her knowledgeable input during my practical work and explaining, as well as assisting in challenging tasks.

I am grateful to Ing. Jana Nebesářová, Csc. for allowing me to conduct my experiments in her laboratory. Furthermore, I want to express my gratitude towards the entire team of the Laboratory of Electron Microscopy.

I would also like to express my gratitude towards Prof. RNDr. Libor Grubhoffer, CSc., Hon. D.Sc., dr. h.c. and Univ.-Prof. Mag. Dr. Dr.h.c. Norbert Müller for establishing the Biological Chemistry study program.

Further I want to thank my parents and friends for the financial and emotional support during my studies.

Abstract

Uranyl acetate (UA) has been used as a heavy metal EM stain for the past 60 years (Bernhard, 1968). Unfortunately, due to rising danger of nuclear warfare, uranium based materials have been heavily regulated, as well as experienced bans throughout the world (Inoue, Muranaka, Park & Yasuda, 2016). In order to find non-radioactive alternatives for UA, different laboratories have investigated the staining ability of other heavy metal containing compounds (Ikeda, Inoue, Kanematsu, Horiuchi & Park, 2010; Inoue, Muranaka, Park & Yasuda, 2016). Here, hafnium chloride ($HfCl_4$) was used as a heavy metal stain under cryogenic conditions. As a model organism unfed *Ixodes ricinus* salivary glands were used, which were high pressure frozen and freeze substitution was performed in the presence of OsO_4, thiocarboydrazide and later $HfCl_4$. For comparison, additional salivary glands were stained with UA using the same freeze substitution protocol. To investigate the staining patterns, ultrathin sections were prepared, counterstained and imaged using a JEOL 1010 TEM. The obtained images show clear staining differences between $HfCl_4$ and UA. UA stained sections showed increased contrast of most cellular structures. $HfCl_4$, on the other hand, showed intense staining of microtubules in myoepithelial cells. Moreover, it appears that $HfCl_4$ stains granules in certain parts of the salivary gland more aggressively, damaging the surrounding tissue and creating artefacts.

Table of Content

Abbreviations

BSA - Bovine serum albumin

CCD - Charge-coupled device

EM - Electron microscopy

ER - Endoplasmic reticulum

EtOH - Ethanol

FS - Freeze substitution

GdAc - Gadolinium triacetate

HEPES - (4-(2-hydroxyethyl)-1-piperazineethanesulfonic acid

HPF - High pressure freezing

$HfCl_4$ - Hafnium tetrachloride

LC - Lead citrate

LaB_6 - Lanthanum hexaboride

NaOH - Sodium hydroxide

OsO_4 - Osmium tetroxide

SEM - Scanning electron microscopy

$SmCl_3$ - Samarium trichloride

ssTEM - Serial section transmission electron microscopy

TCH - Thiocarbohydrazide

TEM - Transmission electron microscopy

UA - Uranyl acetate

YAG - Yttrium-aluminum garnet

1. Introduction

1.1 Electron Microscopy

Electron microscopy is a microscopy technique said to have been first established in Germany by a team of physicists in the 1930ies (von Ardenne,1938; Mulvey, 1967). The until this day operational company Siemens, at that time known as Siemens-Schuckert, held the first patent for magnetic and electrostatic electron lenses for electron microscopy (Marton, 1994). Electron microscopy is based on the principle of an electron beam being used for depicting the image of a specimen or material under vacuum conditions. (Vernon-Parry, 2000; Méndez-Vilas & Díaz, 2007; Abdullah & Mohammed, 2019). It functions due to electrons having a much shorter wavelength than visible light, as well as the resolution increasing if the electrons are at higher speed, which is feasible by increasing the acceleration voltage (Flegler, Heckman, Klomparens, 1993). Commercially available light microscopes can magnify a specimen up to the factor of 1000, while electron microscopes can achieve a magnification of 100,000 to 500,000 times, which corresponds to a resolution well below the one nanometer scale, whereas light microscopes yield resolutions around 200 nm and over (Méndez-Vilas & Díaz, 2007; Vale, Correia, Matos & de M., 2010).

Electron microscopy is separated into two divisions, Scanning Electron Microscopy (SEM), as well as Transmission Electron Microscopy (TEM). The principles of SEM can be expressed as reading the surface of a specimen, by scanning an electron beam across the sample and documenting the scattering of electrons In SEM, an electron counter, such as a scintillator detector, detects backscattered electrons, electrons stemming from the reaction of the electron beam and the specimen, and / or emitted secondary electrons. Backscattered electrons stem from elastic interactions between deeper set sample regions and the beam, while secondary electrons stem from inelastic collisions of the surface and its counterpart. The detected electron signals are composed of either the number of backscattered electrons, which is proportional the atomic number of elements present in the specimen or of secondary electrons attracted to a positively charged faraday cage containing the detector.

1.2 Principles of Transmission Electron Microscopy

In biology, TEM has been used for the past 75 years to image cellular structures and organelles (Porter, Claude & Fullam, 1945). In contrary to SEM, in which a voltage of below 30 kV is used, a voltage of 80 – 300 kV is generally used in TEM, where an electron beam is transmitted through the specimen. For the electron beam to be able to pass through, the sample has to be thinned (Rukari & Babita, 2013; Ilitchev, 2019). In TEM, resolution as precise as 50 pm can be achieved (Erni, Rossell, Kisielowski & Dahmen, 2009). In some cases, even individual atoms can be imaged and thereby details at atomic level can be determined (Fitting Kourkoutis, Plitzko & Baumeister, 2012; Ilitchev, 2019). In biology, for various analyses of cell components, TEM is vital due to its comparatively high resolution and is used to image cells, cell fractions or macromolecules (Hayat, 2000). In biological samples, under-focus is often times used for contrast enhancement, whereby distortion correction is often needed. (Kaynig, Fischer, Müller & Buhmann, 2010). Protein ultrastructures at close to atomic level resolution have been made visible in the past years (Cortese, Diaspro & Tacchetti, 2009).

In TEM, the electron beam can be emitted thermionically into vacuum from a small filament tungsten or microscopic LaB_6 crystal, which is connected to a high voltage source (Kobayashi et al., 1992; Rukari & Babita, 2013). Also, field emission is a possible mode, where a strong electrostatic field is used to induce electron emission. Therein, upon running voltage, the electron source emits primary electrons into vacuum (Rukari & Babita, 2013; Ilitchev, 2019). The beam electrons are focused and positioned by the magnetic field of an objective lens. By also applying electrostatic fields, the angle through which electrons deflect constantly can be adjusted and the electron beam can be shifted. For magnifying, the amount of current flowing through the lenses, needs to be changed. All in all, TEM microscopes incorporate three different lens-classes, one for condensation of the primary electron beam to a fine spot, one for focusing the beam that strikes the sample, and one for expanding the beam for hitting the imaging device accurately. Those imaging screens are usually phosphor based, but also film or YAG screens with CCD cameras are available (Barbe, 1980; Krivanek & Mooney, 1993).

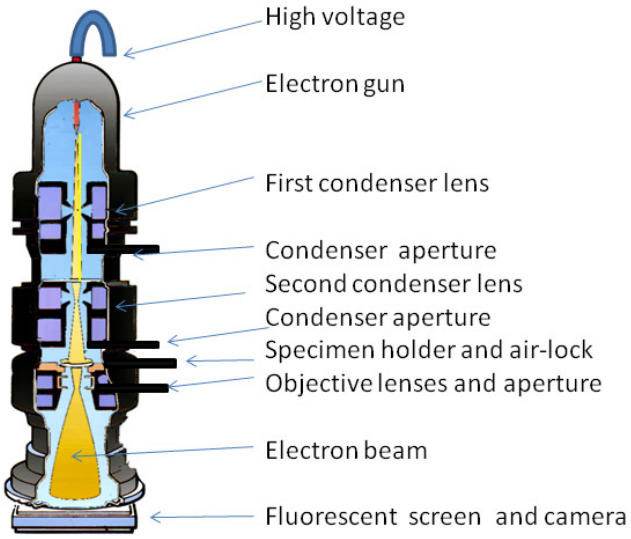

Figure 1: Components of a Transmission Electron Microscope. Adapted from (" The Transmission Electron Microscope | CCBER", 2020)

1.3 Volume Electron Microscopy

Volume Electron Microscopy was initially developed and used to image parts of the central nervous system in order to better the reconstruction when it comes to 3D data of tissue obtained. It was found that due to the small dimensions of synaptic vesicles, great resolution in the z-axis was obtained (Denk & Horstmann, 2004). The 3D data stems either from Serial Section TEM (ssTEM), which incorporates the collecting and imaging of ultrathin sections subsequently cut from the resin sample block. ssTEM is therefore only performed by skilled technicians, because it is necessary to avoid the loss of a section or the creation of artefacts, such as holes, fold overs and stretching of the section (Harris et al., 2006). Another TEM approach to volume EM, yielding 3D data, is called tilt-series tomography, in which projection images are acquired from a section at different tilt angles in regards to the electron beam (from – 70° to +70°) in order to later reconstruct the objects within this section. Also serial images are taken to later be reconstructed into a 3D image and is sometimes repeated across serial sections to examine larger volumes, while still ensuring high resolution (Hoppe, 1981; McEwen & Marko, 2001).

1.4 Biological Specimen Preparation for TEM

Biological materials, analyzed with TEM, need to be manipulated to preserve the cell's structure in native conditions (Fitting Kourkoutis, Plitzko & Baumeister, 2012). These

processes, are called fixing and need to be specifically tailored, to what type of tissue or cells are to be imaged (Cortadellas, Garcia & Fernández, 2010).

With the aim to preserve structure close to native conditions, water can be immobilized by cryofixation (as explained in more detail in chapter 1.5 Cryoimmobiliztion) (Maaz, 2015). Chemical fixation of the biological sample can be performed by fixing the sample with aldehydes in buffer solution at a concentration of 0.1 M. This is followed by postfixation, dehydration with organic solvents and resin embedding.

Historically, the mainly used fixative, long before EM was invented, was formaldehyde (37% w/w) in aqueous solution (formalin), Formalin first needs to be monomerized to methane diol / formaldehyde at pH 7,4 in order to be useable as a fixative for biological tissues, since formaldehyde in water forms polymers (paraformaldehyde) (Pearse, 1980). This monomerization is depicted in figure 2.

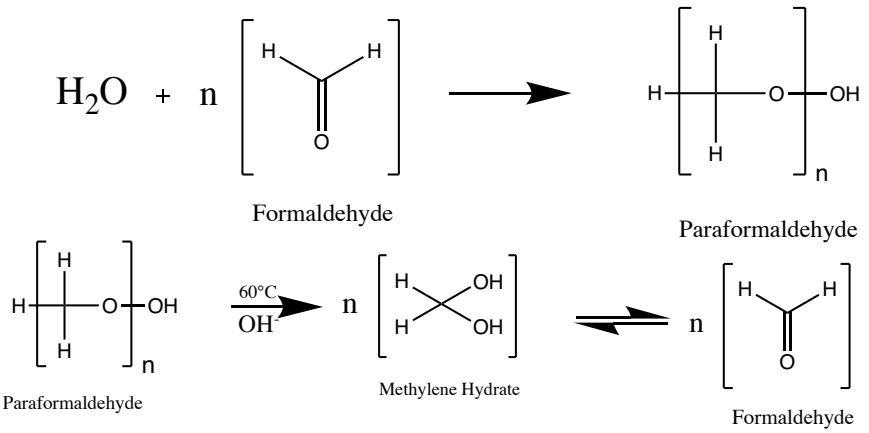

Figure 2: Monomerization of Paraformaldehyde. As proposed by Pearse, 1980.

For EM fixation, low formaldehyde concentrations (0.5% -5%) were used for many years (Hopwood, 1970). As of now, buffered 5% formaldehyde solutions are often times used as a specimen fixative. This is done, since proteins were found to crosslink more efficiently at higher concentrations. At these concentrations, hydrated formaldehyde forms polyoxymethylene glycol by polymerization of methylene hydrate (methylene glycol). The number of monomers polymerized increases with rising formaldehyde concentration (Griffiths, 1993).

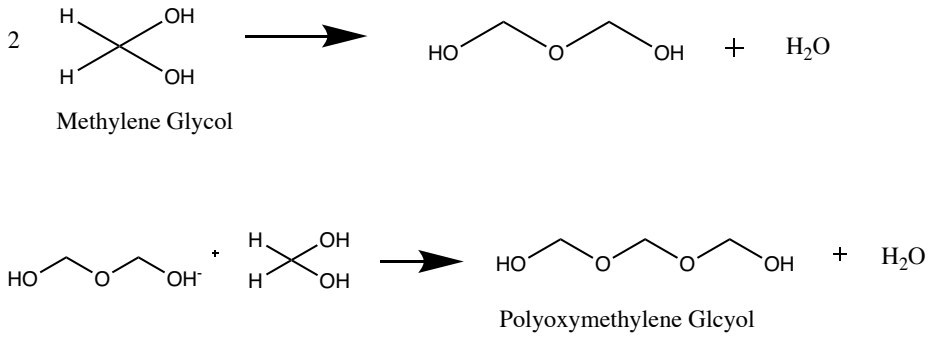

Figure 3: Polymerization to Polyoxymethylene Glycol at High Formaldehyde Concentrations. As proposed by Griffiths, 1993.

In the fixing process, the aldehyde forms methylene bridges with nitrogen atoms. These crosslinks most often occur between the aldehyde and the nitrogen in the basic side group of lysine or with the nitrogen atom in amide bonds between different amino acids, and is depicted in figure 4. With increasing fixation time, the number of methylene bridges increases (Gustavson, 1956).

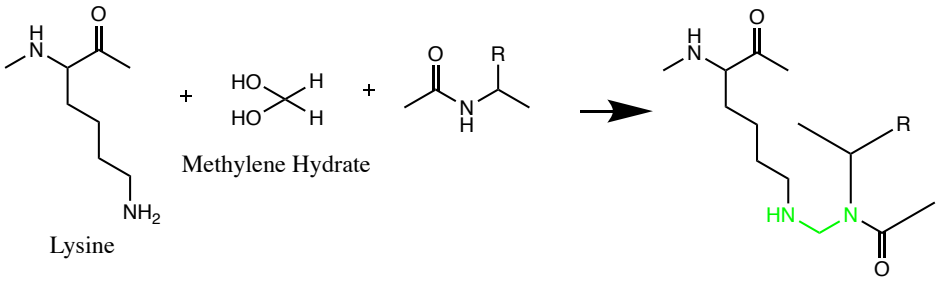

Figure 4: Lysine and Amide Bond of an Amino Acid Crosslinked by Methylene Bridge (green). As proposed by Gustavson, 1956.

Non-proteinogenic substances, such as lipids, carbohydrates and nucleic acids, are not chemically changed by formaldehyde, if the fixation process does not exceed several weeks, which is never the case. These substances are encased in a matrix of crosslinked, insolubilized proteins (Helander, 1994).

In contrary to formaldehyde, glutaraldehyde has two aldehyde functionalities per molecule and therefore shows higher crosslinking potential. As formaldehyde, glutaraldehyde is overly present as a polymer in aqueous solution. But in this case, the polymer has one aldehyde per

repeating unit free to react, as well as one on each end of the polymer, which again showcases the high crosslinking potential. But in order to fit in as many crosslinks as possible and have the molecules penetrate the tissue faster, monomerized glutaraldehyde should be used for the fixation process (Monsan, Puzo & Mazarguil, 1975).

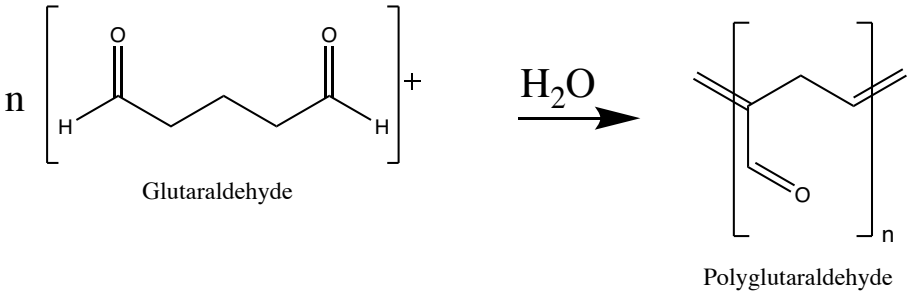

Figure 5: Polymerization of Glutaraldehyde in Aqueous Solution. As Proposed by Monsan, Puzo & Mazarguil, 1975.

Glutaraldehyde crosslinks to free NH_2 groups of amino acids as well as other kinds of nitrogen atoms present in proteins, but does this via imine formation, as explained in figure 5 (Monsan, Puzo & Mazarguil, 1975).

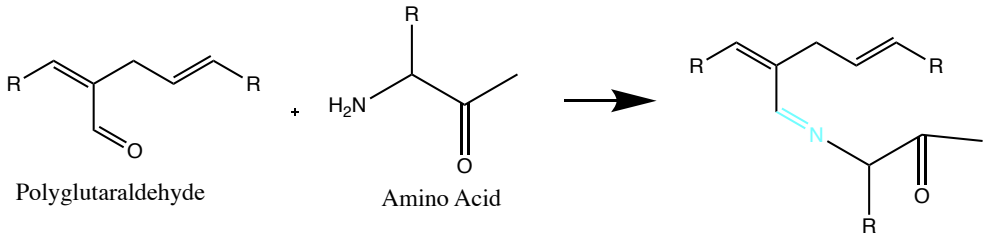

Figure 6: Crosslinking by Glutaraldehyde to Amino Acid via Imine Formation (teal). As proposed by Monsan, Puzo & Mazarguil, 1975.

From this method arose the *Tokuyasu Technique*, in which fixation is performed with 4 % formaldehyde and 0,1 - 0,5 % glutaraldehyde for approximately 1-3 h, dependent on sample thickness. Additionally, the fixed tissue samples are to be stored at 4°C in a 0,1 M phosphate buffer to increase fixation efficiency. In order to infiltrate the samples before freezing, the samples are placed in a glucose or sucrose phosphate buffer solution in an ice bath for up to 30

min, wherein the molar concentration of the sucrose is 2,3 M. Fixed and infiltrated samples are then to be frozen on liquid nitrogen (Tokuyasu, 1973; Griffiths et al., 1984).

1.5 Cryoimmobilisation

Cryofixation is the rapid freezing of the sample in order to avoid the formation of crystals destroying the structure (Dubochet et al., 1988; Cortadellas, Garcia & Fernández, 2010). It is a widely used method for biological TEM sample preparation, since it solidifies the liquid without the presence of crystals, due to the fast cooling (Dubochet, 2007). The basis of this process is known as vitrification (Dubochet et al., 1988). Since this cryo immobilization is instantaneous, the organelles and even the ion gradients in the cytoplasm appears unaltered (Dahl & Staehelin, 1989; McDonald & Auer, 2006). Cryofixation is usually performed for objects with depths up to 200 nm via the process of High Pressure Freezing (HPF) (Moor & Riehle, 1968).

High pressure freezing is based on Le Chatelier's principle, which states, that the volume of water increases upon freezing (Dahl & Staehelin, 1989). Since an increase in volume is unwanted, due to the fact that it would distort all cell components, freezing at elevated pressure assures that the volume increase is held to a minimum. Additionally, it also hinders the formation of crystals in the cells. When no crystals are formed, less heat needs to be extracted per cooling time and the temperature of the total cooling rate, needed for sufficient freezing, is not as low (Studer et al., 1995).

Before and during HPF, the sample is in a 2,1 bar overpressure environment. The freezing is facilitated by a pressurized liquid nitrogen stream that hits the sample, and freezes the sample for approximately 20 milliseconds. After the process, the pressure and temperature are brought up to atmospheric properties (Vanhecke & Struder, 2009).

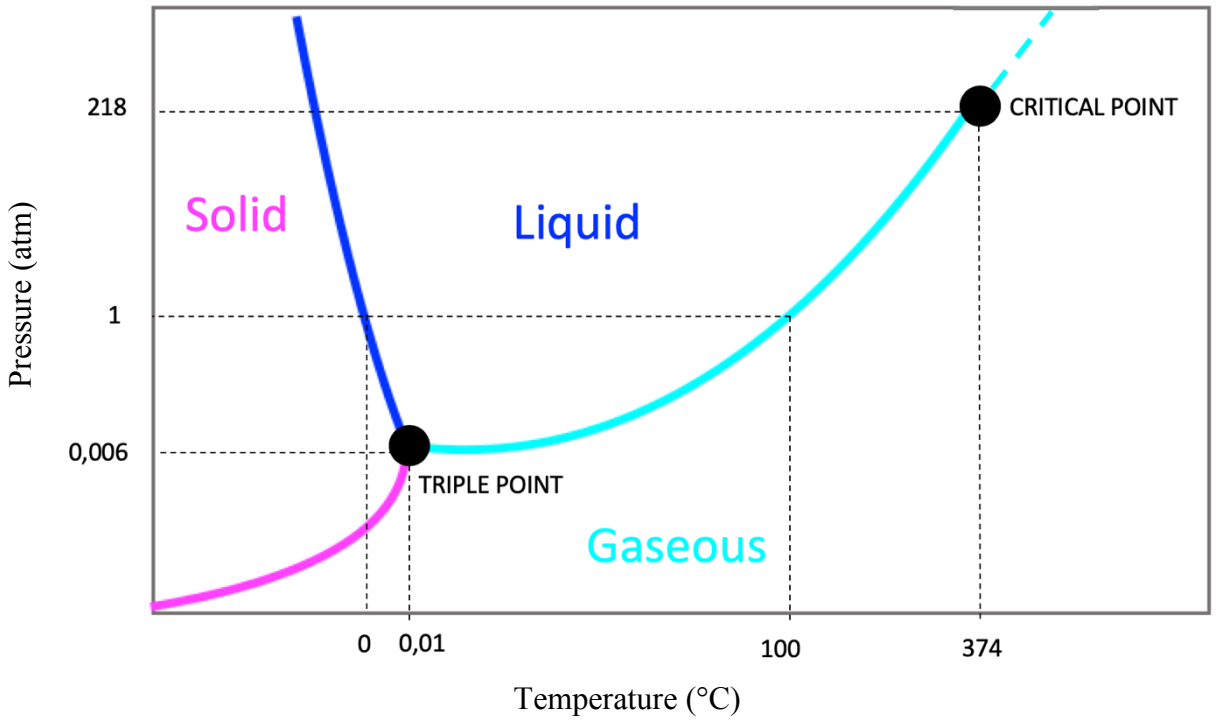

Figure 7: Phase Diagram of Water, modified according to ("Water Phase Diagram | Socratic", 2020)

As the pressure is doubled from the atmospheric 1,013 bar, to 2,1 bar, the freezing temperature is lowered to approximately -92°C (Kanno, Speedy & Angell, 1975; Dahl & Staehelin, 1989). This can be seen in the phase diagram of water depicted in figure 7. Additionally, the melting point of water is also lowered to approximately -22°C (Kanno, Speedy & Angell, 1975).

1.6 Cryosubstitution

In the process following HPF, Freeze Substitution (FS), the biological samples are incubated in chemical fixation agents dissolved in organic solvents below the freezing point of water (Fernandez-Moran, 1960; Bobik, Dunlap & Burch-Smith, 2014). In most cases, the solvent used is either acetone or methanol, while the fixative is OsO_4 in ensemble with UA or glutaraldehyde. The incubation is performed at temperatures ranging from -80 to -90°C. The sample is usually incubated for several days. FS facilitates the substitution of the ice, present in the cells, by the organic solvent together with the fixative. As for the solvent, acetone can be used for quicker FS applications, up to 96 h FS. Methanol is not used in quick FS. The temperature program set, warms up the sample stepwise and during each period the sample is usually incubated in is OsO_4 and UA (as is described more detailed in 1.6.1 OsO_4 Staining), dealing with OsO_4 staining under cryogenic conditions.

In FS, temperature protocols usually require a number of days to be completed, while, as of now, also quicker protocols exist by the name of (super) quick freeze substitution (QFS / SQFS), which are also able to achieve a qualitatively high result (McDonald & Webb, 2011). Additionally, there are methods which incorporate a mixture of different fixation agents, in order to better the visualization of cellular structure, often used in structural research or in research in the field of immunolocalization (Maaz, 2015).

1.6.1 OsO_4 Staining

OsO_4 postfixation is standardly used for the preparation of biological specimen for both TEM, as well as SEM as a secondary fixative of lipids (Prileschajew, 1909; Stoeckenius & Mahr, 1965; Seligman, Wasserkrug & Hanker, 1966). Even though heavy metal staining has not yet been fully understood. Upon binding, OsO_4 oxidizes unsaturated double bonds in fatty acids and is thereby reduced to electron dense metallic osmium. Metallic osmium appears black on the tissue and thereby is used as a secondary stain. In volume EM, strong contrast for bio-membranes is needed. Therefore a method is needed to attract more osmium to one binding site. OsO_4 staining has often been done by following the principle of the OTO-Staining (OsO_4 – TCH – OsO_4 Staining) protocol, where the fixation process initiated by OsO_4 is aided by the usage of Thiocarbohydrazide reacting with the oxide (Seligman, Wasserkrug & Hanker, 1966). By treating the OsO_4 fixated in the sample, with an excess of TCH (1% TCH in aqueous solution) the TCH binds to the OsO_4 in the sample tissue. After, as the name suggests, the sample is treated again with 2% OsO_4 and binds to the TCH sites. This mechanism is called bridging and increases the contrast in the entire tissue, but especially in the cellular structures, that are able to bind the most OsO_4, which generally are membrane lipids. In the original OTO – method staining with hot TCH and OsO_4 vapor was suggested, in order to achieve the best contrast. The OTO-Method is an especially well established one, since it is not said to bring along the loss of lipids in cellular structures, such as droplets and lipoproteins.

In figure 8, the theoretical reactions and subsequent product formation in the first step of OTO – staining is depicted. Firstly, OsO_4 oxidizes a double bond of an unsaturated lipid side chain in a [3+2] cycloaddition to form a cyclic osmate(VI) diester (Prileschajew, 1909; Stoeckenius & Mahr, 1965; Seligman, Wasserkrug & Hanker, 1966). In the second step, TCH binds via alkylation the amino group (*Mannich Reaction*) and with TCH in excess, it is able to bind to

the OsO_4 again via a second amino alkylation, where two possible products can be expected (Mannich & Krösche, 1912; Seligman, Wasserkrug & Hanker, 1966).

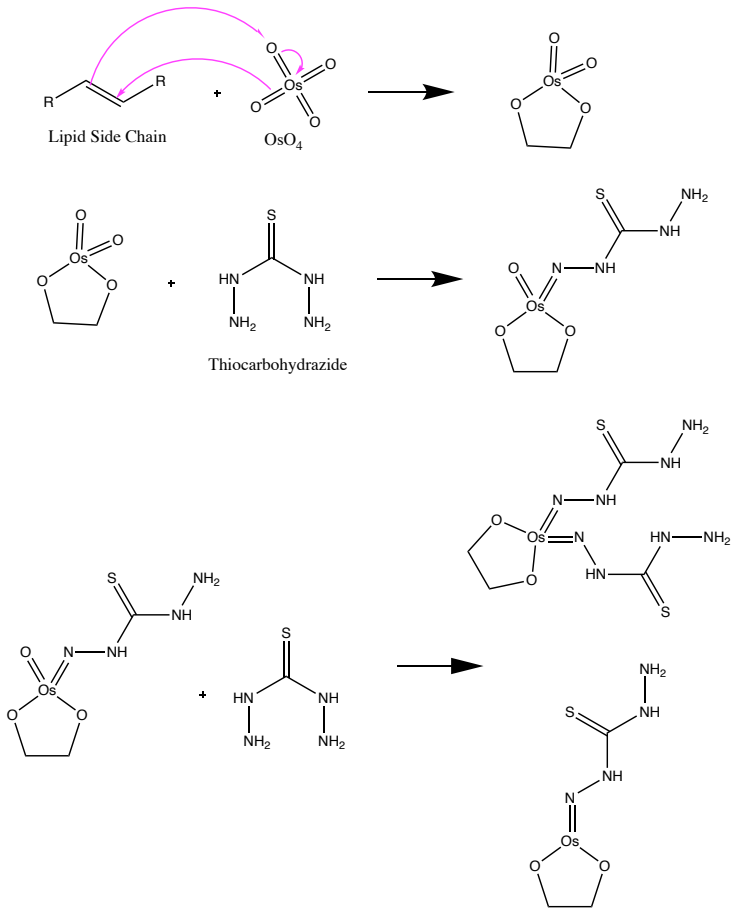

Figure 8: Theoretical Reactions of Lipid Side Chain with OsO_4 and TCH, as proposed by Seligman, Wasserkrug & Hanker, 1966

This results in two products that are due to their structure and deprotonateable Hydrogen atoms on the amino group very likely to attract and bind further OsO_4 and thereby increasing the contrast in membranous structures such as cristae, lipid droplets and vesicles (Seligman, Wasserkrug & Hanker, 1966)

Nowadays, OsO_4 staining under cryogenic conditions, to capture the best possible condition of the tissue, is preferred. OsO_4 has been reported to react already with certain lipids at temperatures as low as – 70°C (White, Andrews, Faller & Barrnett, 1976). Even at temperatures in which OsO_4 is not reactive as a fixative (approximately -90°C) it penetrates the sample. By using OsO_4 at low temperature gradients instead of at room temperature, the formation of

mesosomes, membranous compartments, in for instance stained bacteria is prevented (Ebersold, Cordier & Lüthy, 1981). When at an active temperature, OsO_4 binds to form osmate - Os(VI). This supports the thesis that the initial reaction between an unsaturated lipid and OsO_4 starts at the lipid's double bond to form osmate derivatives, as proposed by Seligman, Wasserkrug & Hanker, 1966. In aqueous medium, via hydrolysis, also more reduced species like Os(IV) and Os(III) are said to be formed and therefore mixtures of these three oxidation states of osmium tetroxide, in the forms of osmate esters, osmium dioxide and in oxo- or amino complexes (Seligman, Wasserkrug & Hanker, 1966).

1.7 Resin Embedding

Polymerizable resin embedding is needed to make the tissue sample suitable for sectioning. For this, either epoxy resin or acrylic resins can be used. Epoxy resins are hydrophobic with Epon or Epon-Araldite being generally the most common Epoxy embedding resins for TEM (Finck, 1960; Carlemalm, Garavito & Villiger, 1982; McDonald, 2014; Jiang & Drummer, 2020). Before initiating the embedding process, the samples need to have undergone complete dehydration with propylene oxide or acetone. When using Spurr's Resin, prior dehydration with ethanol is also possible. After the sample being infiltrated by the chosen resin, the polymerization is facilitated by incubating the sample blocks under heat (Richardson, Jarett & Finke, 1960; Maaz, 2015). Acrylic resins can be infiltrated at either at room temperature or under cold conditions and can be polymerized under UV light at lower temperature or under heat. Sufficient polymerization of the embedding resins requires temperatures of 50°-60°C. They are often used for molecular localization and immunolocalization studies (Carlemalm, Garavito & Villiger, 1982; Jiang & Drummer, 2020).

1.8 Sectioning and Preparing the Sample

Via ultramicotomy, sections of around 60-80nm are sliced off the resin block, which needs to be shaped in a trapezoid way beforehand. The resin block is then trimmed in order to bring the sample to the surface and have an ideal shape for cutting. Grids, 3mm in diameter, are used to support the ultra-thin sections. In order to be able to examine the structure of a tissue, serial sections are often cut and transferred onto grids. These support mesh grids are usually made from copper, nickel or gold and sections can be carbon coated.

1.9 Counter Staining

As a counter stain, UA is the most prevalent chemical, since it is able to fully penetrate the thin sample sections and not just stain the surface (Hayat, 1993). For carbon coated grids, UA is even able to form a staining film on top of the carbon (negative staining), in order to visualize small objects like bacteria, viruses and molecules (Rohde, 2011). This process is done to improve the contrast for highs and lows and increase the signal to noise ratio during imaging (Thompson et al., 2016).

In most laboratories, both UA and lead citrate together are used for counterstaining of resin sections. As for the general staining process, UA interacts with lipids and proteins and thereby enhances the contrast of organelles to cytoplasm, as stated in the UA specific section (Hayat, 1993).

LC interacts with proteins and glycogens for staining purposes. LC interacts with the reduced osmium present in the sample due to fixation and can therefore bind to polar groups in molecules. Additionally, it also reacts with UA and is therefore generally applied to the same sections on the grid, after it was treated with UA (Watson, 1958; Revel, Napolitano & Fawcett, 1960; Reynolds, 1963; Sharma & Sharma, 2014).

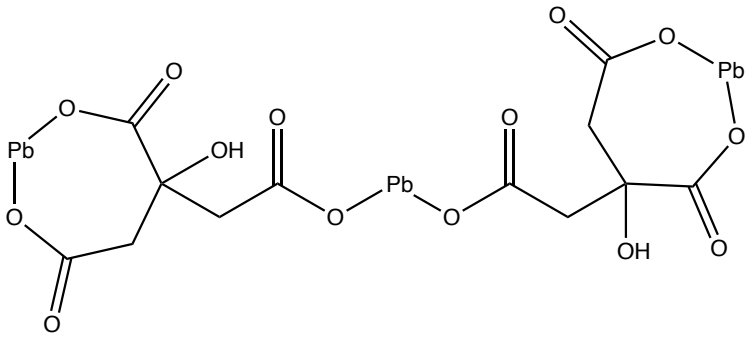

Figure 9: Structure of Lead Citrate, as proposed by "OLED Chemicals ,LCD Chemicals ,Polyimide monomers ,Organic Silanes - Daken Chemical Limited", 2020"

As lead citrate is a chelate compound, depicted in figure 9, and used primarily under strongly basic conditions, it is due to its association constant mainly present as positively charged lead ions, which again have great binding affinity for negatively charged membranous structures,

such as phosphates. These basic lead citrate stains are also less likely to contaminate the sections, as they do not form precipitates when left to stain (Reynolds, 1963).

1.9.1 Problems with the Most Prevalent Staining and Fixating Chemicals

Uranyl acetate, in TEM, is used as a stain and fixative, as well as a counter stain. The UO_2^{2+} ions present in UA, form various complexes, which can bind to positively and negatively charged amino acid sidechains in the biological samples. The binding affinity of these complexes is highly dependent on the surrounding pH, as well as the UA concentration. In TEM, the concentration is often times high enough for the complexes binding to positive groups, to be more likely.

UA, as a uranium derivative, is a radioactive compound. Its most prevalent radioactive emission is in the form of alpha rays. In the EU, uranium containing compounds, fall under the nuclear safeguard mechanism in order to prevent misuse for nuclear weapons (Janžekovič & Križman, 2007). Therefore, in many countries, the purchase of UA is strictly regulated and government controlled, making it difficult to obtain the needed quantities for adequate staining (Inoue, Muranaka, Park & Yasuda, 2016). Additionally to its mild radioactivity, it's acute toxicity and mutagenicity, as well as it being a major environmental hazard, has been a reason for researchers to try to find suitable alternatives for both staining and counter-staining purposes (Inoue, Muranaka, Park & Yasuda, 2016; "Uranyl acetate", 2020; "Uranyl Acetate Technical Data Sheet", 2020).

Using OsO_4 in cooperation with UA, has been shown to increase the readability and contrast of cell and organelle membranes (Hayat, 1993). Therein, uranyl acetate binds to molecules, such as lipids and proteins, containing sialic acid carboxyl groups (Lombardi, Prenna, Okolicsanyi & Gautier, 1971). This is the case in glycoproteins and gangliosides, which are found in the cell membrane`s lipid bilayer (Hayat, 2000; Steck, Yiki & Graus, 2013). Strong interactions with the phosphate backbone of nucleic acids in DNA and RNA have also been reported for UA (Hayat, 2000; Lin, 2020).

The UO_2^{2+} ions are found to be coordinated by four to five oxygen atoms in the carboxylate groups of the amino acids aspartate and glutamate, as well as in anionic nitrates, acetates and

in water molecules (Lin, 2020). Therefore, UA is often present as a dihydrate, as depicted in figure 10.

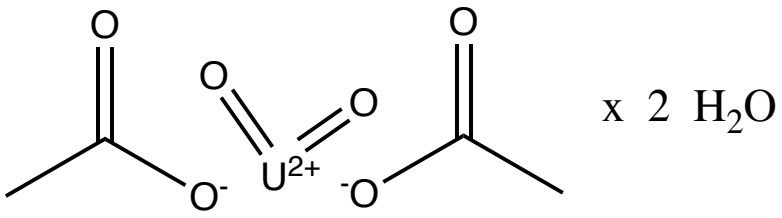

Figure 10: Structure of the Dihydrate of the Acetate Salt of Uranium (UA), as proposed by Pandithage, 2020

The binding mechanism of UA is not just ascribed to the electrostatic cohesion of positive and negative charges, but also due to H-bonds between amino acid side chains or their backbone, with uranyl oxo groups (Lin, 2020). In case of lipids, as in cell membranes, the UO_2^{2+} ion binds to the polar phosphate head group, as depicted in figure 11 (Ting-Beall, 1980; Hayat, 2000).

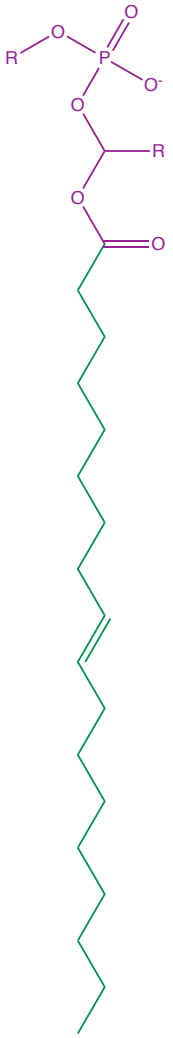

Figure 11: General Structure of a Phospholipid present in Biomembranes, with the Hydrophilic Head Group in Purple and the Hydrophobic (Unsaturated) Fatty Acid Tail in Green.

As a non-radioactive, and therefore easily purchasable alternative to using UA as a heavy-metal EM stain, Inoue, Muranaka, Park & Yasuda, 2016, have explored the possibilities to use $HfCl_4$, $SmCl_3$, and GdAc. The outcome was generally positive. $HfCl_4$ was found to be the superior stain for bio-membranes, $SmCl_3$ for ribosomes and mitochondria and GdAc for cytoskeletal filaments. This fluctuation also indicated that the staining mechanisms behind all three reagents is not the same (Inoue, Muranaka, Park & Yasuda, 2016).

$SmCl_3$ and GdAc are both trivalent lanthanides. Until this point $SmCl_3$ has only been used as a catalyst in organic synthesis (Shen, Huang, Wang & Zhou, 2007). GdAc, on the other hand has been used as a contrasting agent in MRI scans for an extended amount of time, since Gd^{3+} chelates are paramagnetic and water soluble. The magnetic moment generates a localized magnetic field and thereby influences the spin of surrounding protons. It is transported through

the body by lightly binding to serum proteins (Xiao et al., 2016). In the TEM staining mechanism, Gd^{3+} is said to bind to PO_4^{3-} ions, as well as negatively charged protein side chains through ionic bonds (Sherry, Caravan & Lenkinski, 2009).

$HfCl_4$, in contrary to UA, is not present as positively charged ions and the binding process to negatively charged phosphates and carboxylates in membranous structure therefore is not the same (Ikeda, Inoue, Kanematsu, Horiuchi & Park, 2010; Inoue, Muranaka, Park & Yasuda, 2016). $HfCl_4$ is not ionized in organic solvents, but it is thought to form aggregates around the negatively charged parts of membranous structures to which Hf^{4+} binds and stains (Ikeda, Inoue, Kanematsu, Horiuchi & Park, 2010).

Since $HfCl_4$ was found to sufficiently stain bio-membranes, such as cell membranes, nuclear membranes and organelle membranes, as well as good staining for nucleolus, mitochondria, rough ER, glycogen, heterochromatin and even carbohydrates, it seemed to be an all-around adequate alternative for UA (Inoue, Muranaka, Park & Yasuda, 2016). Already in 1984, Hatae, Okuyama & Fujita found $HfCl_4$ to specifically increase the electron density in cytoskeletal elements, such as microtubules, allowing good imaging, showing additional substructural features. Additionally to being a lot easier to purchase, the cost for $HfCl_4$ is over seven times less, as for UA ("Hafnium(IV) chloride", 2020; "Uranyl Acetate EM grade universal stain", 2020).

Problematic in the use of $HfCl_4$ is its hydrolysis to $HfOCl_2$ + HCl in the presence of water (Fang & Dixon, 2013). This happens by leaving a bottle of $HfCl_4$ to react with the moisture in the air and leads to problems in dissolving and staining steps.

1.10 The Importance of Tick Salivary Glands in Research

Salivary glands in hard ticks are not only important for saliva supply, but also for osmoregulation (Kaufman & Philips, 1937). Since ticks feed on blood, excess water and unsuitable ions need to be removed from the feed. This is done via saliva, which contain those unwanted ingredients, and is returned to the host animal. For the species *Ornithodoros moubata*, this is not the case. Their osmoregulatory organ is coxal glands, which are not present in the more common *Ixodes ricinus*.

In *I. ricinus*, the salivary glands are arranged in acini, were types I, II and III are present in female specimen and type IV only in males. Acinus type 1 does not contain any secretory granules and is therefore also called agranular alveoli (Sonenshine & Roe, 2014). Type I acini are composed of four cell types, including a central lamellate cell, constrictor cells, peritubular cells and peripheral cells and are located adjacent to the salivary duct. Type II to IV, granular acini, on the other hand, have a large amount of secretion granules it the cytoplasm. Type II acini consist of 6 cell types, all with granules in hard, and three cell types in soft ticks. The arrangement of the type II acinus cells in hard ticks changes drastically when feeding from a host. Type III acini are the most common type and are structurally similar to type II. Type IV, and only present in male specimen, consist of one granular cell type, as well as two non-granular cell types. They are only present in males, since they are responsible for lubrication and spermatophore transfer to the female in reproduction (Bowman & Sauer, 2004).

Focusing research on tick is vital, not only due to tick-borne diseases threatening to humans but also business wise (Jongejan & Uilenberg, 2004). Tick borne diseases facilitate extensive problems in cattle and other ruminant livestock farming, especially in tick rich areas in Africa, Asia and South America. In less densely tick populated areas, the typical human diseases, such as Lyme Borreliosis and Encephalitis come to mind, which bring along an untypically high mortality rate. As tick salivary glands play a major role in the ticks´ feeding process, studying the structure of them is crucial for understanding and treating tick borne diseases on humans and livestock.

2. Aims

This thesis aims to:

i. Explore the usage of $HfCl_4$ as a heavy-metal TEM stain under cryogenic conditions.

ii. Compare pattern of staining of UA and $HfCl_4$.

iii. Use transmission electron microscopy of salivary glands of *Ixodes ricinus* as a model organism for this comparison.

3. Methods and Materials

3.1 Materials

Chemical	Provider
OsO_4	EMS
TCH	Sigma-Aldrich
UA	EMS
$HfCl_4$	Sigma-Aldrich
Hard Plus Resin	EMS

Table 1: Main Chemicals Used.

3.2 Methods

The samples were prepared in two different batches, batch 1 having been prepared using FS protocol 1 and batch 2 having been prepared using FS protocol 2 (see chapter 3.2.3).

3.2.1 Preparation of Tick Salivary Glands by Tick Dissection

Under a dissecting microscope, unfed ticks were placed onto a wax filled petri dish and by heating up a metal spatula and pressing it into the wax around the tick`s legs, the tick was immobilized. By cutting into the rear end of the tick and along the sides, the dorsal cuticle, as well as the midgut could be removed. The salivary glands are located as grape-like clusters alongside the front legs and are removed by fine tipped forceps (Patton et al., 2012). For fast sample preparation and assuring that cell breakdown could not be visible, the salivary glands were immediately frozen via HPF.

3.2.2 High Pressure Freezing

Via LEICA EM PACT2 (Leica Microsystems), high pressure freezing of the salivary glands were performed. HPF was performed in the presence of BSA in HEPES (20% w/v). Gold plated

copper dishes, containing one salivary gland are inserted into the sample holder and frozen by liquid nitrogen.

3.2.3 Freeze Substitution and Subsequent Staining of Tick Salivary Glands

After successful HPF, the frozen salivary glands in their HPF sample dishes were transferred into 10mL glass vials and placed into the FS chamber of a Leica EM AFS 2. To start the dehydration process, the samples were submerged in solutions specified in table 1 and 2 (all percentages in w/v):

3.2.3.1 FS Protocol 1

Time (h)	Temperature (°C)	Environment
96	- 90	2% OsO_4 in 100% Acetone

This is followed by a temperature rising period of 41h from -90°C to -30°C, with the warming rate being approximately 1,5°C/h.

Time (h)	Temperature (°C)	Environment
24	-30	1% TCH in 100% Acetone
24	-30	2% OsO_4 in 100% Acetone
24	-30	1% UA in 100% Acetone
24	-30	1% $HfCl_4$ in 100% Acetone

Table 2: High Pressure Freezing Protocol for Dehydration and Staining of Tick Salivary Glands from Batch 1

This is followed by a temperature rising period of 24h, going from -30°C to 4°C, with the warming rate being approximately 1.4°C/h.

3.2.3.2 FS Protocol 2

Time (h)	Temperature (°C)	Environment
12	- 90	2% OsO_4 in 100% Acetone

This is followed by a temperature rising period of 12h from -90°C to 10°C, with the warming rate being approximately 8.3°C/h.

Time (h)	Temperature (°C)	Environment
6	-30	1% TCH in 100% Acetone
6	-30	2% OsO_4 in 100% Acetone
18	-30	1% UA in 100% Acetone
18	-30	1% $HfCl_4$ in 100% Acetone

Table 3: High Pressure Freezing Protocol for Dehydration and Staining of Tick Salivary Glands from Batch 2.

This is followed by a temperature rising period of 24h, going from -30°C to 11.3°C, with the warming rate being approximately 1.7°C/h.

Graph 1 depicts the temperature curves for both batches in relation to time spent in the FS chamber.

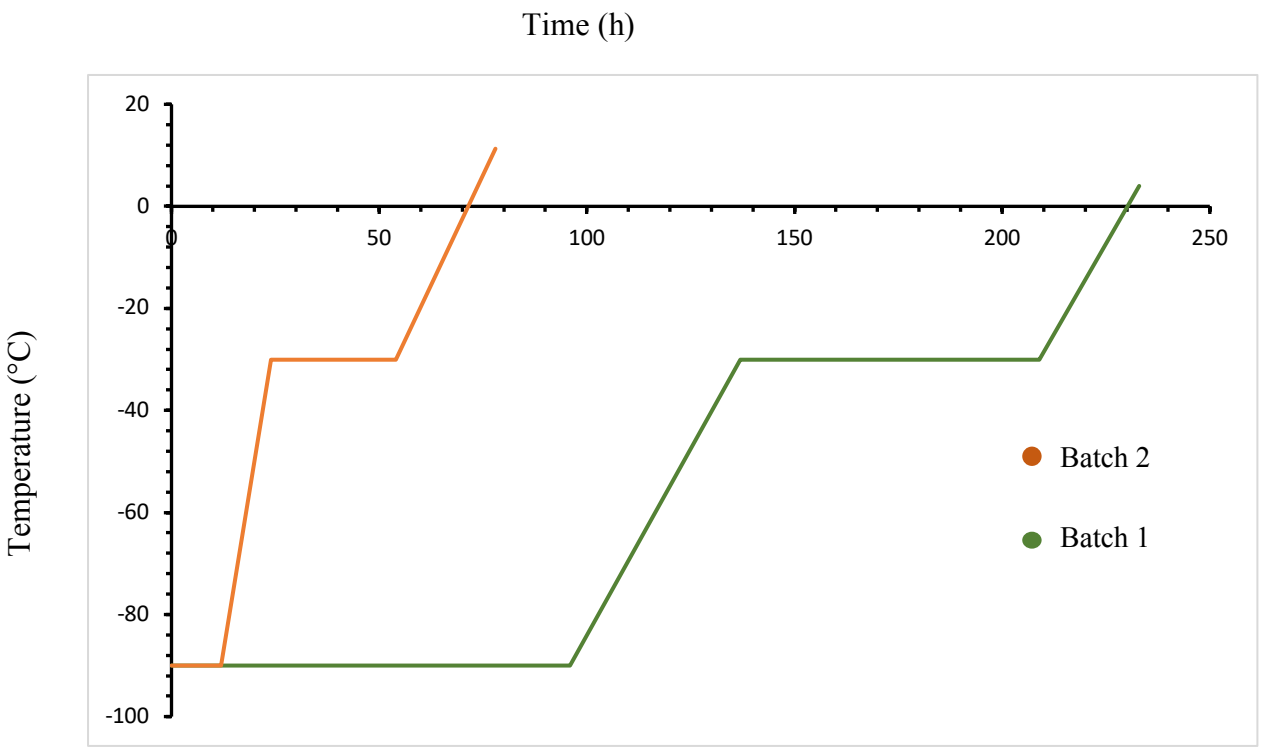

Graph 1: Temperature Curve of both Batches in FS.

Each solution was prepared freshly for use in FS. Solutions containing TCH or UA were covered with aluminum foil during the preparation steps in order to shield them from light to prevent dissociation. Additionally, UA solutions used are pushed through a syringe with a 45 µm pore filter (Merck), to remove crystals. As UA is a radioactive as well as toxic compound, special measurements were taken to ensure laboratory safety. The powdered UA was stored in a fume hood inside a glass bottle kept inside a tin can in order to prevent radioactive emission. At all stages, nitrile gloves were worn and mixing of UA, TCH and OsO_4 solutions was done exclusively under the fume hood. Special radioactive waste compartments were prepared for the disposal of UA solution. Due to its acute toxicity, OsO_4 waste was also collected in separate waste containers.

3.2.4 Resin Infiltration and Embedding

To prepare the samples for resin infiltration, the salivary glands were removed from the HPF discs via pipette and washed with 100% acetone three times for 15 min each, in order to remove any staining agent.

Hard Plus Resin 812 (EMS) was chosen as the resin for the infiltration process, which consists of leaving the dehydrated salivary glands in different resin/acetone mixtures in Eppendorf tubes on a shaker, before putting them into 100% resin for embedding. The specific protocol followed was the same for UA and $HfCl_4$ stained samples and is depicted in table 3.

Time (h)	Environment
1,5	25% Resin in 100% Acetone
1,5	50% Resin in 100% Acetone
1,5	75% Resin in 100% Acetone
12	100% Resin

Table 4: Resin Infiltration Protocol for EMS Hard Plus

The pure resin infiltration was not performed on a shaker, but in a desiccator, to remove any air bubbles that might have been present, since high humidity may disturb the polymerization. After leaving the salivary glands in pure resin overnight, they were embedded in molds and left to polymerize for 48h at 60°C in an incubator oven.

3.2.5 Trimming of Resin Blocks

For sectioning, the polymerized resin blocks were trimmed from the edges by razor blade under the microscope of an ultramicrotome. The rectangular shaped resin blocks were thereby cut into a trapezoid shape.

To prepare the semithin sections, glass knives must be made beforehand. This was done using an LBK Knifemaker, which works on the principle of the balanced break method (Tokuyatsu & Okamura, 1959; Griffiths et al., 1984; "Lkb Glass Knifemaker Manual - Electron Microscopy", 2020). Glass squares were inserted into the holding forks of the knifemaker. Via diamond, a diagonal scratch was made into the glass square and on each side, equal weights pushed down onto the halves. The breaking force used on both sides is equal. After a number of minutes, the glass square snapped in half, revealing one sharp cutting edge knife and a counter piece with a blunt edge. Each knife had a sharp and a blunt side of the blade, depending on the side on top in the knife making process. To have the glass knife collect the semithin sections, a waterproof band was glued around and fixed with gel polish.

The obtained glass knife was then placed in the knife holder of the Leica ultramicrotome and the trapezoid resin block was placed inside the sample holder, facing forward. The space confined between the band and the blade was then filled to the brim with 10% acetone and approximately 200 nm thick, sections were cut from the resin block and collected on acetone. The chosen sections were stained, using a 1% toluidine blue solution, placed on a heating plate at 70 - 80 °C for several seconds and then rinsed with distilled water (Mercer, 1963; Morikawa, Sato & Ezaki, 2018). Under light microscopy, the sections were then examined and if the salivary gland sample was clearly visible, ultrathin sections could be prepared.

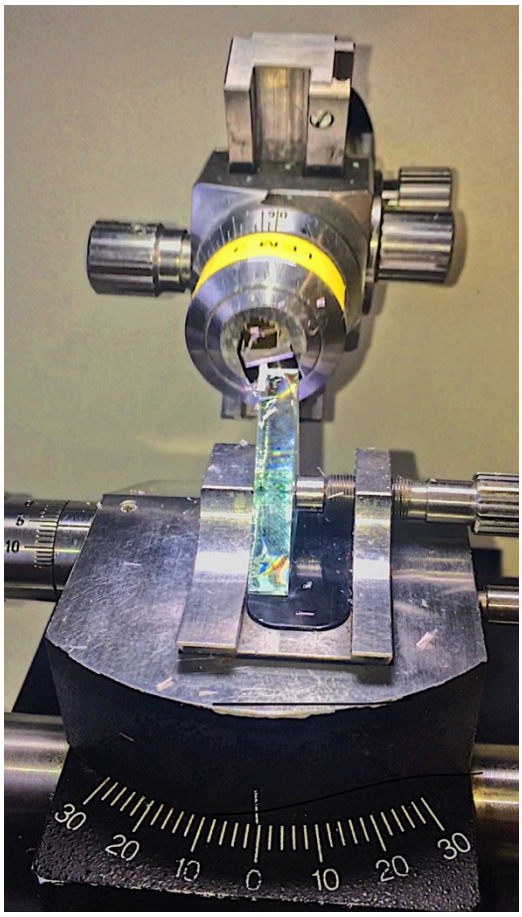

Figure 12: Shaping of Resin Block into Trapezoid via Ultramicrotome.

In order to cut sections thin enough to be used in transmission electron microscopy, diamond knifes were used. Ultrathin sections were cut similarly to the semithin sections, using the ultramicrotome. The sections prepared came out at approximately 50-80 nm in thickness and were collected on a water surface.

After the cutting process, the ultrathin sections were transferred onto copper grids and the upward face was left to dry on filter paper (Yamaguchi & Chibana, 2018).

3.2.6 Counterstaining of the Sections on Grids

For later being able to better distinguish the staining efficiencies of UA and $HfCl_4$ in the OTO-staining process, a number of grids were left not counterstained, others were only counterstained with either UA or LC or with both solutions.

The vessel used for the counterstaining process was a dark chamber, lined with parafilm. In the first step, a saturated ethanolic UA solution was prepared and by weighing in 2.6 g of powdered

UA and dissolving it in an aluminum covered vessel with 20 mL of 50% EtOH for 2 hours with a magnetic stirrer. The obtained solution was filtered through a 0,45 mm syringe filter (Millipore) three times and subsequently stored at 4°C and used within three weeks. For the counterstaining, the solution was again filtered through a 45 μm pore syringe (Merck) and small droplets were placed onto the parafilm in the chamber. The grids were placed sample side down into the droplets. The chamber was then closed, and the grids were left to stain for 20min. Afterwards, the grids were washed for approximately 20 s each in deionized water and placed onto paper, sample facing upwards, to dry. The metal chamber was again lined with parafilm, and a highly concentrated NaOH solution was prepared. Tissue paper were placed into the solution to soak and then the sides of the chamber were lined therewith. This was done to remove carbon dioxide from the atmosphere, as LC would strongly react with it. This is facilitated by a reaction of NaOH and CO_2, to produce Na_2CO_3 and water. LC solution droplets were placed onto the parafilm and the grids were placed, again sample face downwards, into the droplets, the chamber closed and stained for 10min. The stained grids were rinsed with water. After drying, the grids were carbon-coated.

3.2.7 TEM Imaging

All TEM images were made, using a JEOL 1010 TEM, which an operating of 80 kV. Serial sections were produced to provide sufficient ground for comparison between images made.

4. Results

4.1 Specimen Preparation with UA *en-bloc* Staining

UA staining pattern was observed mainly in the myoepithelial cell, basal cells, as well as neck cells surrounding the acinar duct. The myoepithelial cell (one per acinus), which surrounds the lumen of acinus type III , as well as neck cells contain microtubules at high abundances and were therefore an area of interest. Additionally, the staining of cell membranes, the cytoplasm, and substructures of organelles was investigated (Figure 13.A-C.)

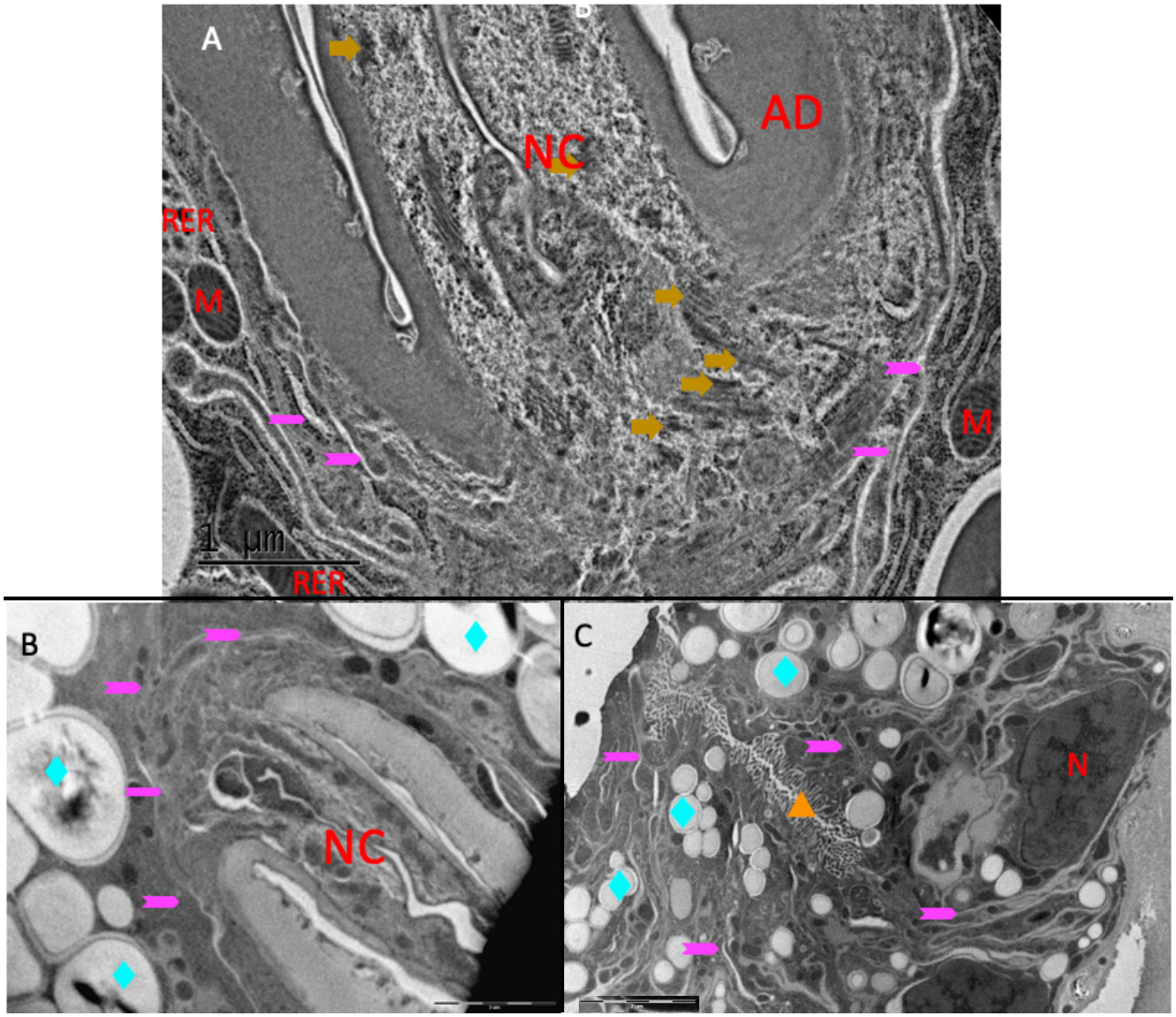

Figure 13: Sections through I. ricinus acinar duct. specimen was en-bloc stained with uranyl acetate according to protocol 1. Images were counterstained with UA and LC respectively and imaged in TEM JEOL 1010. Magenta arrows (cellular membranes of neck cells), beige arrows (microtubules), teal diamonds (granules), orange triangle (acinar lumen). Aveolar duct (AD) and neck cells (NC), mitochondria (M), rough endoplasmic reticulum (RER), nucleus (N). Scale bars: 1µm (A), 2µm (B,C)

In all TEM images in figure 13, typical UA intense cytoplasmic staining pattern was observed. Figure 13.A., at high magnification, depicts the staining and contrast of microtubules in the myoepithelial cell and neck cells, denoted by beige arrows. UA stained microtubules show good contrast and can be distinguished well from the cytoplasm. Also membranes of cellular organelles, denoted by magenta arrows, are depicted nicely. At lower magnification (Figures 13.B. and 13.C.), specific electron densities of the different cell types are observed. Due to high abundance of ribosomes, the electron density in secretory cells was higher than the electron density of other cell types in figures 13.B. and 13.C. Figure 13.B. (enlarged inset) depicts junctions between two basal epithelial cells, denoted with an orange triangle. In all figures, 13.A. – 13.C. the electron density of cellular membranes and the cytoplasm within the specimen appears uniform throughout. As the cytoplasm appears to be stained heavily, a good contrast is created between it and other cellular substructures, in all observed cell types of this area, and therefore enables the imaging of cell membranes, secretory granules, junctions and other structures. In Figures 13.A. and 13.B., the marked cellular membranes most likely belong to basal epithelial cells. As images were taken of granular acini, figures 13.B. and 13.C. show similar acinus type III granular cells, with a different staining pattern. A minimal number of artefacts was noticed.

4.2 Specimen Preparation with $HfCl_4$ *en-bloc* Staining

By investigating the staining pattern of $HfCl_4$ stained salivary glands, two separate staining patters were observed. Firstly, the staining of microtubules in myoepithelial cells and neck cells was described in detail in chapter 4.2.1, as well as the completely electron dense cytoplasm is shown in chapter 4.2.2.

4.2.1 Intense Staining of Microtubules in Neck Cells and Myoepithelial Cell

In the following images (Figure 14.A-F.), intense staining of microtubules in neck cells surrounding the acinar duct can be seen.

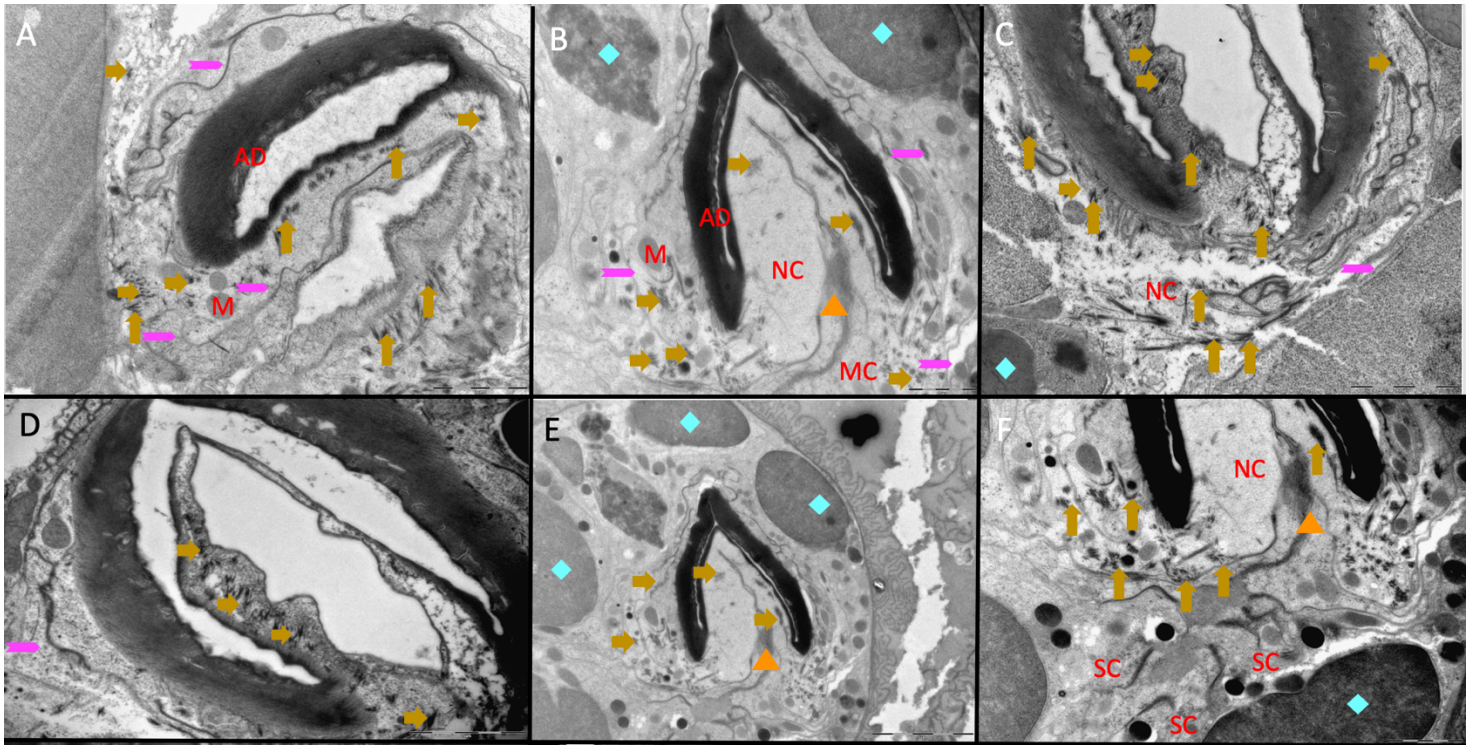

Figure 14: Sections through I. ricinus acinar duct. Specimen was en-bloc stained with hafnium chloride according to protocol 2. Images A,B, E, F were counterstained with UA only, C and D with UA/LC and imaged in TEM JEOL 1010. Magenta arrows (cellular membranes of neck cells), beige arrows (microtubules), teal diamonds (nuclei), orange triangles (epithelial junctions). Alveolar duct (AD), neck cells (NC), mitochondria (M), secretory cells (SC) myoepithelial cell (MC). Scale bars: 2µm (A,B,C, D,F); 5µm (E)

Figure 14.B., and its overview image 14.E. show well stained epithelial junctions between two neck cells and strongly pronounced microtubules within the neck cells, forming the valve. Similar labeling pattern was also observed in the myoepithelial cell, imaged in figure 14.B. (denoted by MC). A neck cell (denoted by NC) with highly pronounced microtubules can be seen in figure 14.F. Organelles, such as mitochondria, display lower contrast. Subjectively, the contrasts of nuclei (as in Figure 14.B. and 14.E.), as well as granules also show less intense contrast.

4.2.2. High Electron-Density of the Cytoplasm of Neck Cells and Myoepithelial Cell

The following images (Figure 15.A-C,F.) depict the electron dense cytoplasm of neck cells and myoepithelial cells, as well as a whole acinus overview (Figure 15.D-E.).

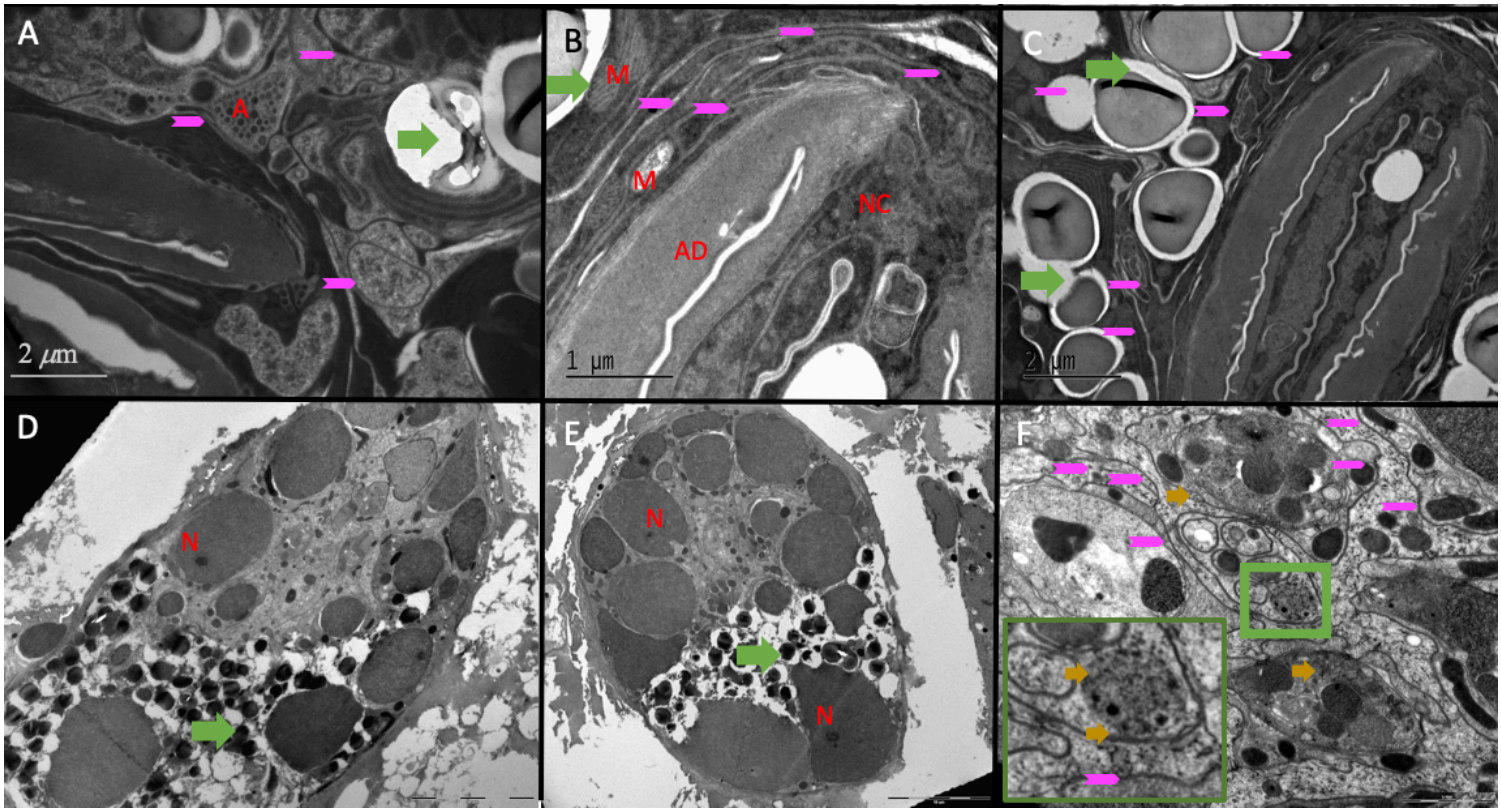

Figure 15: A-C: Sections through I. ricinus acinar duct. D, E: Sections through whole granular acinus. F: Section through myoepithelial and neck cells. Specimen was en-bloc stained with hafnium chloride according to protocol 2. Images were counterstained with UA/LC and imaged in TEM JEOL 1010 . Magenta arrows (cellular membranes), green arrows (artificially electron-lucent area formed around granules). Alveolar duct (AD), valve (V), nucleus (N), neck cells (NC), axons (A). Scale bars: 1 µm (B); 2 µm (A,C,F); 10 µm (D,E). Additionally, image F, shows an enlarged inset, denoted by the green box.

Figure 15.A. shows the high electron-density of the cytoplasm of neck cells and myoepithelial cell. Additionally, it can be seen that axonal projections with their neurosecretory granules are heavily stained (denoted by A). The strongly stained cytoplasm of neck cells are best seen in figures 15.B. and 15.C., wherein also the difference of staining intensity between two unequal acini can be observed. . Therefore, cellular structures, such as microtubules are not visible. An enlarged view into the myoepithelial cell, where cellular structures were visible is given by the inset in figure 15.F. In 15.D. The whole view of an acinus is shown in Fig. 15.E. Artefact formation in the sense of artificially formed empty areas around secretory granules were observed (green arrows in Fig. 15.D and 15.E.).

Interestingly, the staining of nuclei showed also vastly different patterns. In figure 13.C., the nucleus is highly stained and condensed chromatin can be observed, while in figures 15.D. and 15.E., only the nucleolus is seen as an area with higher contrast and no other nuclear compartments can be visualized.

5. Discussion

Uranyl acetate has been used to increase the contrast of biological structures since the 1960s (Bernhard, 1968). It increases the visibility of cell membranes and organelle membranes by binding to the polar phosphate head groups of phospholipid membranes (Ting-Beall, 1980; Hayat, 1993, Hayat, 2000). Unfortunately, heavy restrictions have been placed on uranium derivatives (Inoue, Muranaka, Park & Yasuda, 2016; "Australia's Uranium Export Policy", 2020). Additionally, the high cost and acute toxicity of UA, as well as the logistically extensive radioactive waste disposal problem has fueled the desire to test other ways of heavy metal staining.

$HfCl_4$, as an alternative staining agent, has been tested by a small number of laboratories before, but always under room temperature during sample preparation and subsequent post-staining of the sections (Hatae, Okuyama & Fujita, 1984; Ikeda, Inoue, Kanematsu, Horiuchi & Park, 2010; Inoue, Muranaka, Park & Yasuda, 2016; Vancová et al., 2019). Especially for delicate biological tissue samples, HPF and subsequent staining and dehydration during FS is an essential technique for specimen preparation. To achieve preservation of fine structures of the tissue $HfCl_4$ was investigated by *en bloc* staining during FS, meaning that the findings of this thesis could be of importance for future use of $HfCl_4$ for EM staining.

HPF/FS is nowadays considered to be invaluable for preservation the native structure of biological samples. HPF enables the immobilization of cell structures without crystal formation and fluids inside the cell are fixed to their space in the cell (Dubochet et al., 1988). During cryosubstitution, an organic solvent, containing fixatives are infiltrated into the specimen at low temperatures with the aim to exchange the frozen liquids inside the cells and fixate the cellular structures (Fernandez-Moran, 1960). For microtubules, as an example, it has been shown that HPF, OsO_4 fixation at 40°C, and subsequent FS in the presence of UA improved their visibility, compared to only using OsO_4 fixation (Murata et al., 2002). Excellent staining of microtubules in cultured cells, as well as other cellular substructures such as microfilaments, has also been reported for HPF and subsequent FS, at temperatures starting at -90°C and a subsequent stepwise increase to 0°C. There, the fixation and staining was facilitated by 1% OsO_4 and 0,5% UA in 100% acetone (Shami, Cheng, Henriquez & Braet, 2014).

As a model organism for these experiments, *I. ricinus* salivary glands were used, as they contain various cell types with a large number of microtubules. In general, research focusing on ticks is vital, as livestock worldwide often suffer from lethal tick borne diseases. The salivary glands were high pressure frozen and freeze substitution was performed using the OTO method and subsequent staining with UA in acetone or $HfCl_4$ in acetone was facilitated. Resin infiltration and trimming of the resin block was made before sectioning of the sample. Ultrathin sections were counterstained with UA or UA/LC prior to TEM imaging.

In *I. ricinus*, the neck cells forming the valve are one of the cell types showing a high abundance of microtubules. Additionally, the high electron densities of the cytoplasm of these cells and myoepithelial cells are an interesting feature, as it allows to trace cells in the complicated matrix of the salivary glands.

This very interesting $HfCl_4$ staining pattern is shown in images Fig. 14.B. and 14.C., whereas the UA staining of microtubules was less pronounced (Fig. 13.A.). The microtubules rich myoepithelial cells above the valve contain interesting information regarding the cytoskeleton. This adds to the results stated in Inoue, Muranaka, Park & Yasuda, 2016 as well as Ikeda, Inoue, Kanematsu, Horiuchi & Park, 2010.

The myoepithelial cells above the valve were also imaged in figure 15.F. and show cell membranes, which are heavily stained. In contrast, UA stained image 13.B. shows a highlighted cell membrane, which gives great contrast. Both therefore give good contrast. In regards to basal epithelial cells, images 15.A. and 14.F. ($HfCl_4$), compared with image 13.A. (UA), show better staining of the cell membranes.

From images 14.C. ($HfCl_4$) and 13.A. and 13.B. (UA), it can be deduced that staining differs in the sense that the cytoplasm appears to be stained less heavily for $HfCl_4$ than the cytoplasm stain of UA. Additionally, regarding the cytoplasm's electron density and staining efficiency, counterstaining with lead citrate vastly increases the contrast between cellular structures and the cytoplasm (figures 14.A., 14.F. without LC; 15.C., and 15.A. with LC).

Unfortunately, as depicted in images 15.D. and 15.E., heavy artefact formation around the secretory granules of the acinus was experienced. In figure 15.C. similar artefact formation, even though not as pronounced was also observed. The space separating granules from the

surrounding cytoplasm is most likely due to cytoplasm shrinkage or a site of water drainage during specimen preparation. As the artefact is only in the granulated part of the acinus, one might assume, the chemistry behind $HfCl_4$ staining is not suitable for the preservation of structure of granulated acini and that $HfCl_4$ is subsequently a more aggressive reagent than UA. Moreover, Ikeda, Inoue, Kanematsu, Horiuchi & Park, 2010, experienced different problems when staining with methanolic $HfCl_4$. They dealt with the peeling of the sections from the collodion coated grids, due to the collodions being dissolved. Here, this was not observed, since $HfCl_4$ in 100% acetone was used.

It can be argued that differences in $HfCl_4$ staining pattern and reproducibility of staining can lead to problems when observing, for example, serial sections or tissues in larger volume (serial block-face SEM). As HfCl4 appears to show a slightly irregular staining pattern, it might be challenging to get an identical stain throughout all hundreds of sections needed for ssTEM. Moreover, a regular and fully thorough staining pattern is wanted to ensure later transformation into a full 3D model. Therefore, UA staining can most likely not be replaced by $HfCL_4$ for volume EM techniques. Also, the high density of cytoplasm stained with $HfCL_4$ may interfere with observations of small objects when the thickness of individual ssTEM sections should stay low in the z-axis, as for instance during the examination of small structures. As stated in Harris et al., 2006, sections should not be cut thicker than 50 nm to prevent the overlap of synaptic vesicles or axonal and astroglial processes. The question is if there is a way to improve the staining pattern through chemistry, but investigating this goes beyond this the scope of this thesis..

The staining mechanism of heavy metal stains has not yet been able to be completely explained by science. For uranyl acetate, is assumed that the species dissociates inter alia into bivalently positively charged $(UO_2)^{2+}$ species, which then ionically bind to negatively charged molecules in the specimen (such as phosphates, carboxylates, sulfides and more) (Hayat, 2000). The staining mechanism of $HfCl_4$ is thought to differ. Ikeda, Inoue, Kanematsu, Horiuchi & Park, 2010, suggested that hafnium chloride aggregates are formed from which Hf^{4+} ions emerge and thereby bind to the before stated anions in the specimen.

The use of $HfCl_4$ as an alternative staining agent has arisen out of bans and import restrictions of different countries in regards to radioactive and especially uranium based materials, as stated in earlier (Inoue, Muranaka, Park & Yasuda, 2016). Additionally, it needs to be assured that

said uranium derivatives cannot be used for the development of atomic bombs or in any other types of military programs. Thereby providers of uranium compounds select countries based on their treaty signatures and alliance memberships, as well as their previous history in regards to war and unlawful military actions ("Australia's Uranium Export Policy", 2020).

In nuclear power plants, as well as for the creation of atom bombs and other nuclear weapons, uranium, as it is found in nature cannot be used, since the natural abundancies of uranium isotopes are 99,3% of U^{238} and 0,7% of U^{235}. For the production of nuclear fuel rods, a U^{235} percentage of 3-4 is needed, while approximately 90% U^{235} is needed in order to build an atom bomb. Therefore the process of uranium enrichment has been developed, wherein the mass difference of the two isotopes is used in order to separate them. At high angular velocity in a centrifuge, the heavier U^{238} atoms tend to aggregate to the outside, while the lighter U^{235} atoms can be collected from the inner part. The process is then repeated with all inner atoms for a certain number of times in order to ensure high isotopic purity. Uranyl Acetate, for the usage in EM, on the other hand, is usually U^{235} depleted, meaning that only around 0,3% of the uranium used is of that isotope. As U^{238} is non-fissile, and less radioactive, it is safer for use and also cheaper, as it often is the byproduct of uranium enrichment. (Hore-Lacy, 2016; "Uranyl Acetate Technical Data Sheet", 2020).

With that being said, $HfCl_4$ is, as stated in the introduction, also a lot more affordable than UA ("Hafnium(IV) chloride", 2020; "Uranyl Acetate EM grade universal stain", 2020). Both are sufficient reasons for testing, whether $HfCl_4$, or other non-radioactive stains, are a good alternative for UA in EM staining under cryogenic conditions.

Recently, an additional non-radioactive staining technique, in which a novel synthesized cyclometalated iridium (III) complex (cIr-Tub) was used for probing microtubules in correlative fluorescence spectroscopy and electron microscopy, has been proposed by Tian et al., 2020. In their experiments, the monitoring of the cell dynamics and structure of microtubules was the focus. The principle behind this probe is the metal to ligand charge transfer. Thereby, a molecular orbital charge shift from the metal-like molecular orbitals, to the ligand-like molecular orbitals, takes place, resulting in the oxidation of the metal in the center facilitating fluorescence. When the probe is internalized by selective insertion into microtubules, fluorescent emission is basically switched on. The probe was shown to be able to tag microtubules and can thereby be used for observing cell mitosis. The probe was also

tested to achieve great contrast in different EM methods. When comparing solely OsO_4 postfixed sections with others treated with both OsO_4 and cIr-Tub, the latter showed complex networks of microtubules, while the former did not visualize any microtubules. Following cIr-Tub tagged microtubules could be used for cell tracing and fully understanding the role of microtubules in living systems (Tian et al., 2020).

6. Conclusion

In order to investigate the possibility of $HfCl_4$ as an alternative for UA in TEM staining under cryogenic conditions (HPF – FS), tick salivary glands were stained with either $HfCl_4$ or UA in 100% acetone, sectioned, and counterstained by UA or UA and LC. The imaging was focused on the staining of microtubules, basal epithelial cells and the myoepithelial cell. The results showed sufficient staining for both the standard UA protocol, as well as $HfCl_4$ for the most part. The main difference being the staining pattern of the cytoplasm, which, in contrary to UA, showed a dissimilar staining pattern in different $HfCl_4$ stained acini. On the other hand, the staining of microtubules in neck and myoepithelial cells was excellent for $HfCl_4$ stained sections. Problematic for using $HfCl_4$ in the future is primarily the irregular staining pattern, which would lead to problems in result reproducibility. In addition to this, artefact formation around secretory granules was experienced. But it can be said that $HfCl_4$ could be used particularly for the tracing of myoepithelial cells, by following patterns of heavily stained microtubules, or by examining the highly electron-dense cytoplasm present in the myoepithelial cell, in order to identify the cell's long protrusions surrounding the secretory cells. The $HfCl_4$ staining protocol introduced in these experiments is likely to have limited usage for volume EM techniques.

7. References

Abdullah, A., & Mohammed, A. (2019). Scanning Electron Microscopy (SEM): A Review. *Proceedings Of International Conference On HYDRAULICS, PNEUMATICS, SEALING ELEMENTS, TOOLS, PRECISION MECHANICS, SPECIFIC ELECTRONIC EQUIPMENT & MECHATRONICS*, 1-8.

Ardenne, M. (1938). Das Elektronen-Rastermikroskop. Z. Physik 109, 553–572. https://doi.org/10.1007/BF01341584

Australia's Uranium Export Policy. (2020). Retrieved 30 September 2020, from https://www.dfat.gov.au/international-relations/security/non-proliferation-disarmament-arms-control/policies-agreements-treaties/Pages/australias-uranium-export-policy

Barbe, D. F. (1980). Charge-coupled devices. Vol.38. New York: Springer-Verlag

Bernhard, W. (1968). Une methode de coloration regressive a l'usage de la microscopie electronique. *C. R. Hebd. Static. Acad. Se*, *267*, 2170-2173.

Bobik, K., Dunlap, J. R., & Burch-Smith, T. M. (2014). Tandem high-pressure freezing and quick freeze substitution of plant tissues for transmission electron microscopy. *Journal of visualized experiments : JoVE*, (92), e51844. https://doi.org/10.3791/51844

Bowman, A., & Sauer, J. (2004). Tick salivary glands: function, physiology and future. Parasitology, 129(S1), S67-S81. doi: 10.1017/s0031182004006468

Carlemalm, E., Garavito, R., & Villiger, W. (1982). Resin development for electron microscopy and an analysis of embedding at low temperature*. *Journal Of Microscopy*, *126*(2), 123-143. doi: 10.1111/j.1365-2818.1982.tb00362.x

Cortadellas N, Garcia A, Fernández E. Transmission electron microscopy in cell biology: Sample preparation techniques and image information. Handbook of instrumental techniques from CCiTUB. TEM Cell Biol. 2010, pp 1-11.

Cortese, K., Diaspro, A., & Tacchetti, C. (2009). Advanced Correlative Light/Electron Microscopy: Current Methods and New Developments Using Tokuyasu Cryosections. *Journal Of Histochemistry & Cytochemistry*, *57*(12), 1103-1112. doi: 10.1369/jhc.2009.954214

Dahl, R., & Staehelin, L. (1989). High-pressure freezing for the preservation of biological structure: Theory and practice. *Journal Of Electron Microscopy Technique*, *13*(3), 165-174. doi: 10.1002/jemt.1060130305

Denk, W., & Horstmann, H. (2004). Serial Block-Face Scanning Electron Microscopy to Reconstruct Three-Dimensional Tissue Nanostructure. *Plos Biology*, *2*(11), e329. doi: 10.1371/journal.pbio.0020329

Dubochet J. (2007). The physics of rapid cooling and its implications for cryoimmobilization of cells. Methods in cell biology, 79, 7–21. https://doi.org/10.1016/S0091-679X(06)79001-X

Dubochet, J., Adrian, M., Chang, J., Homo, J., Lepault, J., McDowall, A., & Schultz, P. (1988). Cryo-electron microscopy of vitrified specimens. *Quarterly Reviews of Biophysics, 21*(2), 129-228. doi:10.1017/S0033583500004297

Ebersold, H. R., Cordier, J. L., & Lüthy, P. (1981). Bacterial mesosomes: method dependent artifacts. *Archives of microbiology*, *130*(1), 19–22. https://doi.org/10.1007/BF00527066

Erni, R., Rossell, M., Kisielowski, C., & Dahmen, U. (2009). Atomic-Resolution Imaging with a Sub-50-pm Electron Probe. *Physical Review Letters*, *102*(9). doi: 10.1103/physrevlett.102.096101

F. Vale, A.C. Correia, B. Matos, J. M. N. and A. P. A. de M. (2010). Applications of transmission electron microscopy to virus detection and identifcation. Microsc. Sci. Technol. Appl. Educ. A. Méndez.

Fang, Z., & Dixon, D. (2013). Hydrolysis of ZrCl4and HfCl4: The Initial Steps in the High-Temperature Oxidation of Metal Chlorides to Produce ZrO2and HfO2. The Journal Of Physical Chemistry C, 117(15), 7459-7474. doi: 10.1021/jp400228d

Fernandez-Moran H. (1960). Low-temperature preparation techniques for electron microscopy of biological specimens based on rapid freezing with liquid helium II. Annals of the New York Academy of Sciences, 85, 689–713. https://doi.org/10.1111/j.1749-6632.1960.tb49990.x

Finck, H. (1960). Epoxy Resins in Electron Microscopy. The Journal Of Biophysical And Biochemical Cytology, 7(1), 27-30. doi: 10.1083/jcb.7.1.27

Fitting Kourkoutis, L., Plitzko, J., & Baumeister, W. (2012). Electron Microscopy of Biological Materials at the Nanometer Scale. *Annual Review Of Materials Research*, *42*(1), 33-58. doi: 10.1146/annurev-matsci-070511-155004

Griffiths, G. (1993). *Fine Structure Immunocytochemistry* (1st ed., p. 37). Heidelberg: Springer-Verlag Berlin Heidelberg.

Griffiths G, McDowall A, Back R et al (1984) On the preparation of cryosections for immunocytochemistry. J Ultrastruct Res 89:65–78

Gustavson KH. (1956). The chemistry of tanning processes. 1st ed. New York: Academic Press; Aldehyde tanning; pp. 244–82.

H. Kobayashi et al., Emittance Mearsurement for High-Brightness Electron Guns, 1992 Linear Accelerator Conf., Ottawa, Canada, August 1992.

Hafnium(IV) chloride. (2020). Retrieved 26 May 2020, from https://www.sigmaaldrich.com/catalog/product/aldrich/258202?lang=de&region=AT

Harris, K., Perry, E., Bourne, J., Feinberg, M., Ostroff, L., & Hurlburt, J. (2006). Uniform Serial Sectioning for Transmission Electron Microscopy. *Journal Of Neuroscience*, *26*(47), 12101-12103. doi: 10.1523/jneurosci.3994-06.2006

Hatae, T., Okuyama, K., & Fujita, M. (1984). Visualization of the Cytoskeletal Elements in Tissue Culture Cells by Bloc-Staining with Hafnium Chloride after Rapid Freezing and Freeze-Substitution Fixation. *Journal Of Electron Microscopy*, *33*(2), 186-190. doi: 10.1093/oxfordjournals.jmicro.a050456

Hayat, M. (1993). *Stains and Cytochemical Methods* (pp. 354-355). Springer Science & Business Media.

Hayat, M. (2000). Principles and techniques of electron microscopy: biological applications. 4th edn. 543pp. Cambridge: Cambridge University Press. £65 (hardback). Annals Of Botany, 87(4), 546-548. doi: 10.1006/anbo.2001.1367

Helander, K. (1994). Kinetic Studies of Formaldehyde Binding in Tissue. *Biotechnic & Histochemistry*, *69*(3), 177-179. doi: 10.3109/10520299409106282

Hoppe W. (1981). Three-dimensional electron microscopy. *Annual review of biophysics and bioengineering*, *10*, 563–592. https://doi.org/10.1146/annurev.bb.10.060181.00

Hopwood, D. (1970). Cell and tissue fixation. *The Histochemical Journal*, *17*(4), 389-442. doi: 10.1007/bf01003203

Hore-Lacy, I. (2016). *Uranium for nuclear power* (1st ed., pp. 321-351). Woodhead Publishing Elsevier Ltd.
https://doi.org/10.1016/B978-0-444-52902-2.00011-4

Ikeda, K., Inoue, K., Kanematsu, S., Horiuchi, Y., & Park, P. (2010). Enhanced effects of nonisotopic hafnium chloride in methanol as a substitute for uranyl acetate in TEM contrast of ultrastructure of fungal and plant cells. Microscopy Research And Technique, n/a-n/a. doi: 10.1002/jemt.20964

Ilitchev, A. (2019). Transmission (TEM) vs. Scanning (SEM) Electron Microscopes: What's the Difference? - Accelerating Microscopy. Retrieved 4 April 2020, from https://www.thermofisher.com/blog/microscopy/tem-vs-sem-whats-the-difference/

Inoue, K., Muranaka, Y., Park, P., & Yasuda, H. (2016). Exploration of non-radioactive alternative stains to uranyl acetate. *In European Microscopy Congress 2016: Proceedings, (Ed.)*. doi:10.1002/9783527808465.EMC2016.6065

Janžekovič, H., & Križman, M. (2007). Radioactive Sources in Chemical Laboratories. *Proceedings Of The International Conference Nuclear Energy For New Europe, Portorož, Slovenia, Sept. 10-13, 2007*.

Jiang, F., & Drummer, D. (2020). Curing Kinetic Analysis of Acrylate Photopolymer for Additive Manufacturing by Photo-DSC. *Polymers*, *12*(5), 1080. doi: 10.3390/polym12051080

Jongejan, F., & Uilenberg, G. (2004). The global importance of ticks. Parasitology, 129(S1), S3-S14. doi: 10.1017/s0031182004005967

Kanno, H., Speedy, R. J., & Angell, C. A. (1975). Supercooling of Water to -92{degrees}C Under Pressure. Science (New York, N.Y.), 189(4206), 880–881. https://doi.org/10.1126/science.189.4206.880

Kaufman, W. R. & Phillips, J. E. (1973). Ion and water balance in the Ixodid tick Dermacentor andersoni: III. Influence of monovalent ions and osmotic pressure on salivary secretion. Journal of Experimental Biology 58, 549–564.

Kaynig, V., Fischer, B., Müller, E., & Buhmann, J. M. (2010). Fully automatic stitching and distortion correction of transmission electron microscope images. *Journal of structural biology*, *171*(2), 163–173. https://doi.org/10.1016/j.jsb.2010.04.012

Krivanek, O., & Mooney, P. (1993). Applications of slow-scan CCD cameras in transmission electron microscopy. Ultramicroscopy, 49(1-4), 95-108. doi: 10.1016/0304-3991(93)90216-k

Lin, Y. (2020). Uranyl Binding to Proteins and Structural-Functional Impacts. *Biomolecules*, *10*(3), 457. doi: 10.3390/biom10030457

Lkb Glass Knifemaker Manual - Electron Microscopy. (2020). Retrieved 25 July 2020, from https://www.barnardhealth.us/electron-microscopy-2/introduction-yzn.html

Lombardi, L., Prenna, G., Okolicsanyi, L., & Gautier, A. (1971). Electron staining with uranyl acetate possible role of free amino groups. *Journal Of Histochemistry & Cytochemistry*, *19*(3), 161-168. doi: 10.1177/19.3.161

Maaz, K. (2015). *The transmission electron microscope*. Rijeka, Croatia: InTech. doi:10.5772/59457

Mannich, C., & Krösche, W. (1912). Ueber ein Kondensationsprodukt aus Formaldehyd, Ammoniak und Antipyrin. Archiv Der Pharmazie, 250(1), 647-667. doi: 10.1002/ardp.19122500151

Marton, L. (1994). Early history of the electron microscope (pp. 1-32). San Francisco, Calif.: San Francisco Press.

McDonald K. L. (2014). Rapid embedding methods into epoxy and LR White resins for morphological and immunological analysis of cryofixed biological specimens. Microscopy and microanalysis : the official journal of Microscopy Society of America, Microbeam Analysis Society, Microscopical Society of Canada, 20(1), 152–163. https://doi.org/10.1017/S1431927613013846

McDonald, K. and Webb, R. (2011), Freeze substitution in 3 hours or less. Journal of Microscopy, 243: 227-233. doi:10.1111/j.1365-2818.2011.03526.x

McEwen, B., & Marko, M. (2001). The Emergence of Electron Tomography as an Important Tool for Investigating Cellular Ultrastructure. Journal Of Histochemistry & Cytochemistry, 49(5), 553-563. doi: 10.1177/002215540104900502

Méndez-Vilas, A., & Díaz, J. (2007). *Modern research and educational topics in microscopy* (pp. 122-131). Badajoz: Formatex.

Mercer, E.H. (1963), A SCHEME FOR SECTION STAINING IN ELECTRON MICROSCOPY. Journal of the Royal Microscopical Society, 81: 179-186. doi:10.1111/j.1365-2818.1963.tb02089.x

Monsan, P., Puzo, G., & Mazarguil, H. (1975). Étude du mécanisme d'établissement des liaisons glutaraldéhyde-protéines. *Biochimie*, *57*(11-12), 1281-1292. doi: 10.1016/s0300-9084(76)80540-8

Moor H, Riehle U. (1968). Snap-freezing under high pressure: A new fixation technique for freeze-etching. Proc 4th Eur Reg Conf Electron Microsc. 2, 33–4.

Morikawa, S., Sato, A., & Ezaki, T. (2018). A simple, one-step polychromatic staining method for epoxy-embedded semithin tissue sections. Microscopy (Oxford, England), 67(6), 331–344. https://doi.org/10.1093/jmicro/dfy037

Mulvey, T. (1967). The history of the electron microscope. Proceedings Of The Royal Microscopical Society, 2(1), 207-227.

OLED Chemicals ,LCD Chemicals ,Polyimide monomers ,Organic Silanes - Daken Chemical Limited. (2020). Retrieved 27 July 2020, from http://www.dakentech.com

Murata, T., Karahara, I., Kozuka, T., Thomas Jr., H.G., Staehelin, L.A., Mineyuki, Y. (2002). Improved method for visualizing coated pits, microfilaments, and microtubules in cryofixed and freeze-substituted plant cells. Journal of Electron Microscopy, 51: 133-136.

Pandithage, R. (2020). Brief Introduction to Contrasting for EM Sample Preparation. Retrieved 24 May 2020, from https://www.leica-microsystems.com/science-lab/brief-introduction-to-contrasting-for-em-sample-preparation/

Patton, T. G., Dietrich, G., Brandt, K., Dolan, M. C., Piesman, J., & Gilmore, R. D., Jr (2012). Saliva, salivary gland, and hemolymph collection from Ixodes scapularis ticks. Journal of visualized experiments : JoVE, (60), 3894. https://doi.org/10.3791/3894

PEARSE, A. G. E. (1980). *Histochemistry: Theoretical and Applied*. Vol 1, 2nd edn. Edinburgh: Churchill-Livingstone.

Porter, K. R., Claude, A., & Fullam, E. F. (1945). A STUDY OF TISSUE CULTURE CELLS BY ELECTRON MICROSCOPY : METHODS AND PRELIMINARY OBSERVATIONS. The Journal of experimental medicine, 81(3), 233–246. https://doi.org/10.1084/jem.81.3.233

Prileschajew, N. (1909), Oxydation ungesättigter Verbindungen mittels organischer Superoxyde. Ber. Dtsch. Chem. Ges., 42: 4811-4815. doi:10.1002/cber.190904204100

Revel, J., Napolitano, L., & Fawcett, D. (1960). IDENTIFICATION OF GLYCOGEN IN ELECTRON MICROGRAPHS OF THIN TISSUE SECTIONS. *The Journal Of Biophysical And Biochemical Cytology*, *8*(3), 575-589. doi: 10.1083/jcb.8.3.575

Reynolds, E. (1963). THE USE OF LEAD CITRATE AT HIGH pH AS AN ELECTRON-OPAQUE STAIN IN ELECTRON MICROSCOPY. The Journal Of Cell Biology, 17(1), 208-212. doi: 10.1083/jcb.17.1.208

Richardson, K., Jarett, L., & Finke, E. (1960). Embedding in Epoxy Resins for Ultrathin Sectioning in Electron Microscopy. *Stain Technology*, *35*(6), 313-323. doi: 10.3109/10520296009114754

Rohde, M. *Taxonomy of Prokaryotes*; (2011). Rainey, F., Oren, A., Eds.; Methods in Microbiology; Academic Press. Vol. 38, pp 61– 100.

Rukari, T., & Babita, A. (2013). Review Article TRANSMISSION ELECTRON MICROSCOPY-AN OVERVIEW. *ISSN Online: - 2321-7855 International Research Journal For Inventions In Pharmaceutical Sciences*, *1*(2), 1-7.

Seligman, A., Wasserkrug, H., & Hanker, J. (1966). A NEW STAINING METHOD (OTO) FOR ENHANCING CONTRAST OF LIPID-CONTAINING MEMBRANES AND DROPLETS IN OSMIUM TETROXIDE-FIXED TISSUE WITH OSMIOPHILIC THIOCARBOHYDRAZIDE (TCH). *The Journal Of Cell Biology*, *30*(2), 424-432. doi: 10.1083/jcb.30.2.424

Shami, G.J., Cheng, D., Henriquez, J., Braet, F. (2014). An assessment of high-pressure freezing and freeze substitution protocols of cultured cells. *Microscopy: advances in scientific research and education* (6th ed., p. 10-15) Formatex Research Center.

Sharma, A., & Sharma, A. (2014). *Chromosome Techniques: Theory and Practice* (3rd ed., p. 225). Butterworth-Heinemann.

Shen, Q., Huang, W., Wang, J., & Zhou, X. (2007). SmCl3-catalyzed C-acylation of 1,3-dicarbonyl compounds and malononitrile. *Organic letters*, *9*(22), 4491–4494. https://doi.org/10.1021/ol701961z

Sherry, A. D., Caravan, P., & Lenkinski, R. E. (2009). Primer on gadolinium chemistry. *Journal of magnetic resonance imaging : JMRI*, *30*(6), 1240–1248. https://doi.org/10.1002/jmri.21966

Sonenshine, D., & Roe, R. (2014). Biology of ticks (2nd ed., pp. 163-205). New York, NY: Oxford University Press.

Steck, A., Yiki, N., Graus, F. (2013). Antibody testing in peripheral nerve disorders. *Handbook of Clinical Neurology.* 115, 189-212

Stoeckenius W, Mahr (1965) SC. STUDIES ON THE REACTION OF OSMIUM TETROXIDE WITH LIPIDS AND RELATED COMPOUNDS. Laboratory Investigation; a Journal of Technical Methods and Pathology., 14:1196-1207.

Studer, D., Michel, M., Wohlwend, M., Hunziker, E. B., & Buschmann, M. D. (1995). Vitrification of articular cartilage by high-pressure freezing. *Journal of microscopy*, *179*(Pt 3), 321–332. https://doi.org/10.1111/j.1365-2818.1995.tb03648.x

The Transmission Electron Microscope | CCBER. (2020). Retrieved 5 April 2020, from https://www.ccber.ucsb.edu/collections-botanical-collections-plant-anatomy/transmission-electron-microscope

Thompson, R. F., Walker, M., Siebert, C. A., Muench, S. P., & Ranson, N. A. (2016). An introduction to sample preparation and imaging by cryo-electron microscopy for structural biology. *Methods (San Diego, Calif.)*, *100*, 3–15. https://doi.org/10.1016/j.ymeth.2016.02.017

Tian, X., De Pace, C., Ruiz-Perez, L., Chen, B., Su, R., Zhang, M., Zhang, R., Zhang, Q., Wang, Q., Zhou, H., Wu, J., Zhang, Z., Tian, Y., & Battaglia, G. (2020). A Cyclometalated Iridium (III) Complex as a Microtubule Probe for Correlative Super-Resolution Fluorescence and Electron Microscopy. *Advanced materials (Deerfield Beach, Fla.)*, e2003901. Advance online publication. https://doi.org/10.1002/adma.202003901

Ting-Beall, H.P. (1980), Interactions of uranyl ions with lipid bilayer membranes. Journal of Microscopy, 118: 221-227. doi:10.1111/j.1365-2818.1980.tb00264.x

Tokuyasu K, Okamura S (1959) A new method for making glass knives for thin sectioning. J Biophys Biochem Cytol 6:305–308

Tokuyasu, K. (1973). A TECHNIQUE FOR ULTRACRYOTOMY OF CELL SUSPENSIONS AND TISSUES. *The Journal Of Cell Biology*, *57*(2), 551-565. doi: 10.1083/jcb.57.2.551

Uranyl Acetate EM grade universal stain. (2020). Retrieved 26 May 2020, from http://www.agarscientific.com/uranyl-acetate-25g

Uranyl Acetate Technical Data Sheet. (2020). Retrieved 23 May 2020, from https://www.emsdiasum.com/microscopy/technical/datasheet/22400.aspx

Uranyl acetate. (2020). Retrieved 23 May 2020, from https://pubchem.ncbi.nlm.nih.gov/compound/Uranyl-acetate#section=GHS-Classification

Vancová, M., Bílý, T., Nebesářová, J., Grubhoffer, L., Bonnet, S., Park, Y., & Šimo, L. (2019). Ultrastructural mapping of salivary gland innervation in the tick Ixodes ricinus. *Scientific Reports*, *9*(1). doi: 10.1038/s41598-019-43284-6

Vanhecke D, Studer D (2009) High pressure freezing Leica EM PACT. In: Cavalier A, Spehner D, Humbel BM (eds) Handbook of cryo-preparation methods for electron microscopy. CRC, Boca Raton, pp 129–156

Vernon-Parry, K. (2000). Scanning Electron Microscopy: an introduction. *III-Vs Review*, *13*(4), 40-44.

Water Phase Diagram | Socratic. (2020). Retrieved 24 July 2020, from https://socratic.org/questions/how-does-the-water-phase-diagram-differ-from-those-of-most-substances

Watson, M. (1958). Staining of Tissue Sections for Electron Microscopy with Heavy Metals. *The Journal Of Biophysical And Biochemical Cytology*, *4*(6), 727-730. doi: 10.1083/jcb.4.6.727

White, D., Andrews, S., Faller, J., & Barrnett, R. (1976). The chemical nature of osmium tetroxide fixation and staining of membranes by X-ray photoelectron spectroscopy. *Biochimica Et Biophysica Acta (BBA) - Biomembranes*, *436*(3), 577-592. doi: 10.1016/0005-2736(76)90442-9

Xiao, Y., Paudel, R., Liu, J., Ma, C., Zhang, Z., & Zhou, S. (2016). MRI contrast agents: Classification and application (Review). International Journal of Molecular Medicine, 38, 1319-1326. https://doi.org/10.3892/ijmm.2016.2744

Yamaguchi, M., & Chibana, H. (2018). A Method for Obtaining Serial Ultrathin Sections of Microorganisms in

Transmission Electron Microscopy. Journal of visualized experiments : JoVE, (131), 56235. https://doi.org/10.3791/56235